Quantitative localization of Cav2.1 (P/Q-type calcium channel) in the rat cerebellum

Dwi Wahyu Indriati

DOCTOR OF PHYLOSOPHY

National Institute for Physiological Sciences

School of Life Science

The Graduate University
for Advanced Studies

2013

CONTENTS

1. SUMMARY

This study focuses on P/Q-type voltage-dependent calcium channels, which have roles in transmitter release, integration of dendritic signals, generation of dendritic spikes, and gene expression. These channels found abundantly in the cerebellum. It is important to know the precise localization of these channels along the plasma membrane since high intracellular calcium concentration transient produced by opening of these channels is restricted to tens to hundreds of nanometers from the channels. In order to understand the precise location of $Ca_v2.1$ channel, I used SDS-digested freeze fracture replica labeling (SDS-FRL) method to study channel distribution and quantify the number of $Ca_v2.1$ in the cerebellum. I found 17.1 $Ca_v2.1$ particles on average in a single parallel fiber (PF) active zone, giving the estimated labeling efficiency of 62.6–118% as compare with estimated number of functional channels calculated from previous electrophysiological reports (14.5 to 27.3 functional channels). Localization of $Ca_v2.1$ in the active zone of PF terminals and also CF terminals showed that this channel is not randomly organized but instead concentrated in micro clusters within the active zone. In Purkinje cells (PCs), a high density of $Ca_v2.1$ in spines was revealed in the periphery of postsynaptic density (PSD). In the somatodendritic compartment, I found two distinct patterns of $Ca_v2.1$ distribution, scattered and clustered. The scattered $Ca_v2.1$ had a somatodendritic gradient with 2.5-fold increase in the density of immunogold particles from soma to distal dendrites. The higher number of calcium channesl in the distal dendrite can be one of the reasons for higher and quicker $[Ca^{2+}]i$ changes observed in the fine dendrites compared to the thicker dendrites. The

other population with 74-fold higher density than the scattered particles was found within clusters of intramembrane particles on the protoplasmic face (P-face) of soma and primary dendrites. Both populations of $Ca_v2.1$ were found as early as postnatal day 3 (P3) and increased in the second postnatal week to a mature level in rat. Using double immunogold labeling, I found that virtually all of the $Ca_v2.1$ clusters were co-localized with two types of calcium-activated potassium channels, BK and SK2, with the nearest neighbor distance (NND) of ~40 nm. The calcium nanodomain created by the opening of $Ca_v2.1$ channels likely activates the two channels, which limit the extent of depolarization of PCs.

Previous studies showed that calcium channel β subunits determine the maturation, biophysical properties and cell surface expression of high voltage-dependent channels. It is of interest to know which β subunit is actually the partner of $Ca_v2.1$ in the cerebellum. It is known that β_4 subunit is expressed throughout the cerebellum particularly in the molecular layer, but the role of this subunit in the arrangement of cell surface expression of $Ca_v2.1$ remains elusive. So I focused on investigating the co-localization between these two molecules, $Ca_v2.1$ and β_4 subunits to get the insight of how these two molecules are coupled. I found that $Ca_v2.1$ and β_4 subunits are mostly co-localized in the active zone with NND of ~215 nm. However, I couldn't find any difference in expression and the micro clustering of $Ca_v2.1$ particles within the active zone in β_4 subunit-deficient (lethargic) mice compared with that in WT. Thus it is possible that β_4 subunit doesn't interfere with spatial arrangement of $Ca_v2.1$ in the active zone, or other β subunit(s) can compensate the lack of β_4 subunit in the lethargic mice.

2. INTRODUCTION

It is well known that Ca^{2+} regulates a large variety of cellular process. More than ten thousand-fold calcium concentration gradient exists across neuronal plasma membrane, and openings of voltage dependent calcium channels (VDCCs) allow transient influx of Ca^{2+} that creates a distinct intracellular signal and precisely controls many cellular mechanisms. These Ca^{2+} signaling restricted to a very narrow range due to their characteristic cell structures and intracellular Ca^{2+} diffusion and buffering which is generated by specific and non-specific Ca^{2+}-binding cytosolic protein, thus, mechanisms dependent on such signal must be situated quite close to the site of influx. It is also well known that solely Na^{+} and K^{+} conductances do not dictate the membrane potential dynamics but VDCCs can also contribute. For these reasons, subcellular localization of VDCCs is likely to be strategically arranged. Locations of VDCCs can be electrophysiologically hunted using outside-out patches but only from soma and large processes. Calcium imaging studies have visualized intracellular calcium concentration ($[Ca^{2+}]i$) but with resolution limited to hundreds of nanometer range. Important neuronal functions such as vesicular release depend on $[Ca^{2+}]i$ increase within tens of nanometers from the calcium influx source (calcium nanodomain) and only electron microscopy has this resolution. Here, I used highly sensitive SDS-digested freeze-fracture replica labeling (SDS-FRL) for $Ca_v2.1$ subunit to visualize the two-dimensional distribution of P/Q-type VDCCs along the plasma membrane.

SDS-FRL method was originally developed by Fujimoto (Fujimoto, 1995) to visualize two-dimensional distribution of membrane molecules on freeze-fracture replicas. The tissue is frozen, freeze-fractured, shadowed with platinum–carbon and then replicated using carbon. Then the tissue beneath the replica is dissolved with SDS, leaving the membrane proteins in the carbon-fixed membrane halves. The membrane protein is separated into two; P-face and exoplasmic face (E-face). Antibodies for the intracellular and extracellular domains can be applied to the P-face and E-face, respectively (Fujimoto, 1995).

The advantage of SDS-FRL method over conventional immunogold methods are, first, it has higher sensitivity in detecting membrane proteins because the membrane proteins are exposed on the two-dimensional surface of the replica so it is readily accessible by immunoreagents. Since SDS denatures epitopes, antibodies used for immunoblot analysis can react similarly with proteins immobilized on the replica membrane. Second, SDS- FRL method is more efficient, rapid with the regard to the analysis of a large number of samples and it is highly reproducible than the post-embedding method, which requires laborious and time-consuming reconstruction of serial ultrathin sections. But this method also has several limitations. First, it is often difficult to identify the labeled profiles just based on the morphological features, so it is necessary to label marker proteins to help in identification of the fractured membranes. Second, since fracturing process occurs randomly, the chances of fracturing membranes that have different curvature will be different. It can lead to the difficulty in getting specific target cells and sampling bias in synapse collection. Third, there are also possibilities that certain protein is preferentially allocated to either the P-face or the E-face or other will be allocated to both faces. Thus for quantitative analysis study, careful examination of the allocation of a molecule is needed.

In my study, I applied thin (2nm) coat of evaporated carbon before shadowing with platinum-carbon to increase the detection efficiency and maintain the retention of membrane lipid molecules (Masugi-Tokita et al., 2007; Fujita et al., 2007).

Among the various types of VDCCs, the P/Q-type ($Ca_v2.1$) has a prevailing role in a number of neuronal functions and is most abundant in Purkinje cells (PCs) (Westenbroek et al., 1995). For this reason, I decided to analyze quantitative localization of $Ca_v2.1$ in the cerebellum. The $Ca_v2.1$ channels play key roles in the generation of dendritic spikes (Tank et al., 1988) after climbing fiber (CF) activation (Davie et al., 2008) or strong PF activation (Rancz and Ha¨usser, 2006) and in the amplification of exitatory postsynaptics potentials (EPSPs) in the distal dendrites (De Schutter and Bower, 1994). The $Ca_v2.1$ channels also have indispensable roles in the postnatal development of the cerebellar circuitry. $Ca_v2.1$ fuels heterosynaptic competition between climbing and parallel fibers and also homosynaptic competition among multiple climbing fibers in developing cerebellum (Miyazaki et al., 2004; Hashimoto et al., 2011). Thus in my study it is important to know whether I can detect the labeling of $Ca_v2.1$ in first postnatal week of rat's life.

Calcium imaging studies showed that after burst of spikes in PCs, higher and quicker changes in $[Ca^{2+}]_i$ was seen in thinner dendrite compare to thicker dendrite (Lev-Ram et al., 1992). These events are mostly understood due to the difference in surface-to-volume ratio (Lev-Ram et al., 1992) while $Ca_v2.1$ channel density variation is poorly understood. So it is reasonable to compare the density of $Ca_v2.1$ particles in certain compartments such as, soma, primary dendrite, secondary dendrite and distal dendrite to examine how the $Ca_v2.1$ number variation contribute to the different $[Ca^{2+}]_i$ seen in thinner and thicker dendrites.

Previous studies showed that calcium-activated potassium channels, BK have scattered and clustered distribution patterns as that in PCs (Kaufmann et al., 2009, 2010). It has also been shown that the calcium influx through of $Ca_v2.1$ mainly fuels activation of both BK and SK2 subtypes of K_{Ca} in PC (Womack et al., 2004). Such activation of calcium-activated potassium channel (K_{Ca}) underlies the characteristic after-hyperpolarization following calcium spikes in PCs (Edgerton and Reinhart, 2003) and may result in bidirectional effects on excitability (Montgomery and Meredith, 2012). Effective Ca^{2+}-mediated channel communication requires their assembly in specific subcellular compartments. By electron microscopy, a junctional membrane complex between the cell membrane and the endoplasmic/sarcoplasmic reticulum (ER/SR) has been observed. This structure known as 'plasmerosomes' has been thought to have a function as Ca^{2+}-mediated crosstalk between cell-surface and intracellular channels (Blaustein and Golovina, 2001; Berridge, 2002). Therefore I focused on studying the spatial coupling between $Ca_v2.1$ and K_{Ca} to understand how the activation of K_{Ca} is regulated.

High-voltage dependent calcium channels are composed of four subunits, including α_1, $\alpha_2\delta$, β and γ based on biochemical purification (Catterall, 2000). The α_1 subunit forms the pore of the calcium channel. One of the auxiliary subunits, β subunit interacts directly with α_1 subunit predominantly through a highly conserved Alpha Interaction Domain (AID) in α_1 subunit (Pragnell et al., 1994) and a corresponding Beta Interactio Domain (BID) in β subunit (De Waard et al., 1994). β subunit is the only subunit of the calcium channel that is entirely cytosolic. The β subunit helps in the trafficking of α_1 to the plasma membrane, by its ability to mask an endoplasmic reticulum retention signal in the α_1 subunit (Bichet et al., 2000). Four genes encode the β subunits ($\beta_1 - \beta_4$). All of the 4 genes are expressed in the brain. Although the β subunit has an ability to form heterogeneous complexes with other subunits, it is clear that each type of

VDCCs has a predominant β subunit. For example, β_4 is the predominant subunit associated with the P/Q-type calcium channels, while β_3 is predominantly associated with the N-type calcium channels (Arikkath and Campbell, 2003).

A previous study revealed that the carboxy and amino termini of β_4 subunit allow the localization of the protein to presynaptic sites in cultured hippocampal neurons (Wittemann et al., 2000). The lethargic mice caused by a spontaneous mutation in the gene encoding the β_4 subunit, have truncated β_4 and lack the BID (Burgess et al., 1999). This mutant shows ataxia, lethargic behavior and spontaneous focal motor seizures (Arikkath and Campbell, 2003). In the lethargic mice, the absence of interaction with β_4 doesn't result in any changes in the P/Q-type currents in the Purkinje neurons implying that there is a compensation for the loss of β_4 subunit in electrophysiological function of the channel. However since the compensation is not complete, lethargic mouse still has the severe phenotype. The reason for the lack of compensation may be due to the ability of β_4 subunit to interact specifically with certain cellular proteins that allow specific localization of VDCC to subcellular components. In my study I examined colocalization of $Ca_v2.1$ and β_4 subunit in the presynaptic active zone and alteration of $Ca_v2.1$ expression and distribution in lethargic mice.

3. Materials and Methods

3.1 Ethical Approval

All procedures in this study were performed according to the Guidelines for Care and Use of Laboratory Animals of the Physiological Society of Japan. Experimental protocols were reviewed and approved in advance by the Institutional Animal Care and Use Committee of the National Institutes of Natural Sciences.

3.2 Animals

Wistar rats at postnatal days (P) 3, 7, 14, 21, 28 (n = 3 each for P3-21, n = 4 for P28) and young adults (8 weeks, n = 3), $Ca_v2.1$ knock-out (KO) (donated by Hee-Sup Shin, Center for Cognition and Sociality, Institute for Basic Science, Seoul), adult SK2 KO (donated by Dr. John P. Adelman, Vollum Institute, Oregon), adult BK KO (donated by Dr. Andrea L Meredith, Dept of Physiology, University of Maryland, School of Medicine, Baltimore) and wild-type (WT) mice were used (n= 3 each). The rats and mice were raised on a 12 h light/dark cycle with water and food *ad libitum.* All animal experiments were conducted in accordance with the guidelines of the National Institute for Physiological Science's Animal Care and Use Committee.

3.3 SDS-digested freeze-fracture replica labeling (SDS-FRL)

SDS-FRL was performed with some modifications (Masugi-Tokita & Shigemoto, 2007; Masugi-Tokita et al., 2007; Tarusawa et al., 2009; Kasugai et al., 2010) of the technique developed by Fujimoto (Fujimoto, 1995). The rats were anesthetized with sodium pentobarbital (50 mg/kg,

i.p.) and perfused transcardially with 25 mM PBS for 1 min, followed by perfusion with 2% paraformaldehyde (PFA) and 15% saturated picric acid solution in 0.1 M phosphate buffer (PB) for 12 min. Sagital or coronal slices (130 μm thick) were cut using a vibrating microslicer (Linear-Pro7, Dosaka, Kyoto) in 0.1 M PB. Regions from middle lobules containing granule cell, Purkinje cell, and molecular layers were trimmed from cerebellar slices. The trimmed slices were immersed in graded glycerol of 10-30% in 0.1 M PB at 4°C overnight then rapidly frozen by a high pressure freezing machine (HPM010, BAL-TEC, Balzers).

3.3.1 Somatodendritic, presynaptic and postsynaptic labeling of $Ca_v2.1$

Frozen samples were fractured into two parts at -140°C (-120°C for SK2 KO) and replicated by carbon deposition (2 nm thick), platinum (uni-direction from 60°, 2 nm) and carbon (15 nm) in a freeze-fracture replica machine (JFD II, JEOL, Tokyo). Tissue debris was dissolved with gentle shaking at 80°C for 18 h in a solution containing 15 mM Tris-HCl (pH 8.3), 20% sucrose, and 2.5% SDS. For P3 samples, tissue debris was dissolved in a solution containing 15 mM Tris-HCl (pH 6.8), 20% sucrose and 2.5% SDS. The replicas were washed three times in 50 mM Tris-buffered saline (TBS) (pH 7.4) containing 0.05% bovine serum albumin (BSA) and blocked with 5% BSA in the washing buffer for 1 hour at room temperature. The replicas were then incubated with the guinea pig primary antibody against $Ca_v2.1$ subunit of P/Q-type calcium channel (8 μg/ml) overnight at 15°C followed by incubation with anti-guinea pig secondary antibodies conjugated with 5 nm gold particles (British Biocell International (BBI), Cardiff) overnight at 15°C. The specificity of the $Ca_v2.1$ antibody was confirmed by testing cerebellar tissue from $Ca_v2.1$ KO mice (Jun et al., 1999). Immunogold particles for $Ca_v2.1$ were mostly abolished in the KO tissue (see results). Co-localization of $Ca_v2.1$ with calcium-activated potassium channels was examined with double labeling with rabbit antibodies against BK channel (Kaufmann et al.,

2009; Kauffman, 2010) and SK2 channel (Cueni et al., 2008). For double labeling for $Ca_v2.1$ with BK channel, SK2 channel, vesicular glutamate transporter 1 (vGluT1) or vesicular glutamate transporter 2 (vGluT2) (Neuromab) , replicas were first reacted with the $Ca_v2.1$ antibody (8 µg/ml) and then anti-guinea pig secondary antibody followed by incubation with the BK antibody (4 µg/ml), SK2 antibody (3 µg/ml), vGlut1 antibody (8.3 µg/ml), or vGlut2 antibody (8.4 µg/ml) then anti-rabbit secondary antibody for BK and SK2 or anti-mouse secondary antibody for vGluT1 and vGluT2. For postsynaptic labeling, mix antibody of $Ca_v2.1$ and mGluR1α (1:500 dilution) were applied followed by application of mix secondary antibody, anti-guinea pig secondary antibody conjugated with 5 nm gold particles and anti-rabbit secondary antibody conjugated with 10 nm gold particles. After immunogold labeling, the replicas were rinsed three times with 0.05% BSA/TBS, washed with TBS and distilled water, and picked up onto grids coated with pioloform (Agar Scientific, Stansted, Essex).

3.3.2 Double labeling of $Ca_v2.1$ and β_4 subunits of calcium channel

To increase labeling efficiency for β_4 subunit of calcium channel, which is intracellular protein we performed carbon replica experiment. For carbon replica samples (β_4 subunit labeling), frozen samples were fractured into two parts at -140°C then replicated with carbon deposition (15nm) in freeze-fracture replica machine (JFD II, JEOL, Tokyo). Tissue debris was dissolved with gentle shaking at 80°C for 18 h in a solution containing 15 mM Tris-HCl (pH 8.3), 20% sucrose, and 2.5% SDS. The replicas were washed three times in 50 mM Tris-buffered saline (TBS) (pH 7.4) containing 0.05% bovine serum albumin (BSA) and blocked with 5% BSA in the washing buffer for 1 hour at room temperature. The replicas were first reacted with the guinea pig primary antibody against $Ca_v2.1$ subunit of P/Q-type calcium channel (8 µg/ml) or rabbit primary

antibody against β_4 subunit (8.6 µg/ml, donated by Dr. Yasuo Mohri, Kyoto University, Kyoto) overnight at 15°C followed by incubation with anti-guinea pig secondary antibodies conjugated with 2 nm gold particles or rabbit secondary antibodies conjugated with 2 nm gold particles (British Biocell International (BBI), Cardiff) overnight at 15°C followed by incubation with the β_4 subunit (8.6 µg/ml) antibody or $Ca_v2.1$ subunit of P/Q-type calcium channel antibody (8 µg/ml) then with anti-rabbit secondary antibodies conjugated with 5 nm gold particles or anti-guinea pig secondary antibodies conjugated with 5 nm gold particles overnight at 15°C. After immunogold labeling, the replicas were rinsed three times with 0.05% BSA/TBS, washed with TBS and distilled water, and picked up onto grids coated with pioloform (Agar Scientific, Stansted, Essex).

3.4 Data Analysis

3.4.1 Counting the number of synapse per parallel fiber bouton.

Rats (P17, n = 2) were anesthetized with sodium pentobarbital (50 mg/kg, i.p.) and perfused transcardially with 25 mM PBS, followed by perfusion with 0.8% of PFA and 1.5% of glutaraldehyde in 0.1 M PB (pH 7.4) for 12 min. Coronal sections (50 µm thick) were cut using a vibrating microslicer (VT-1000S, Leica, Wetzlar) in 0.1 M PB. After washing in 0.1 M PB several times, sections were treated with 1% OsO_4 in 0.1 M PB for 1 h, stained with 2% uranyl acetate, dehydrated in graded ethanol, and flat-embedded in Durcupan resin (Fluka, Sigma Aldrich, St. Louis). Serial ultrathin sections were prepared at 70 nm thickness (Ultracut S; Leica) and images of PF boutons were captured from the beginning to the end of each bouton at magnification of 15,000 or 25,000. PF-spine synapses were identified based on asymmetrical

synapses with a terminal containing round loosely aggregated synaptic vesicles (Palay and Chan-Palay,1974).

3.4.2 Measurement of IMP cluster area and quantification of the density of immunogold particles

The labeled replicas were examined using a transmission electron microscope (Tecnai-12; FEI, Oregon) and photographed at magnifications of 13,500, 26,500 and 97,000. The $Ca_v2.1$ antibody used in this study showed labeling concentrated on the protoplasmic face (P-face) of the plasma membrane, whereas no specific labeling was found on the exoplasmic face (E-face). The area of intramembrane particle (IMP) clusters was delineated manually using iTEM software (Olympus Soft Imaging Software, Tokyo). Immunogold particles within 30 nm from the edge of IMP clusters were included in the analysis based on the possible distance of the immunogold particle from the epitope (Matsubara et al., 1996). For the measurement of immunogold particle density, profiles of soma and dendrites were tilted to make then as flat as possible. Background labeling was measured on the P-face of the Purkinje cell soma in $Ca_v2.1$ KO mice.

3.4.3 Measurement of active zone area and quantification of the density of immunogold particles in PF and CF terminal

The labeled replicas were examined using a transmission electron microscope (JEM 1010; FEI, Oregon) and photographed at magnification of 150,000. The $Ca_v2.1$ antibody used in this study showed labeling concentrated on the protoplasmic face (P-face) of the plasma membrane, whereas no specific labeling was found on the exoplasmic face (E-face). The area of presumably active zone which is looked as concave shape was delineated manually using iTEM software

(Olympus Soft Imaging Software, Tokyo). Labeling of vGluT1 and vGluT2 were used for differentiating PF and CF terminals. For the measurement of immunogold particle density, tilting was adjusted to capture PF and CF profiles with maximum areas for better size estimation of presynaptic active zone. Background labeling was measured on the P-face of the PF terminal in $Ca_v2.1$ KO mice.

3.4.4 Analysis of spatial distance between $Ca_v2.1$ and calcium activated-potassium channels.

The XY coordinates for 5 nm gold particles ($Ca_v2.1$) and 10 nm gold particles (either BK or SK2) were plotted using iTEM software. Using a macro written in-house for the Excel software, we measured the nearest neighbor distances (NNDs) between the 5 nm gold particles and the 10 nm gold particles. Distances between the two particles were then compared with those between the real $Ca_v2.1$ and the random BK or SK2 distributions. Random distributions were generated by first counting the number of BK or SK2 in each profile. Then, the same number of particles was distributed randomly within the same delineated area of the IMP cluster. In the real distributions, we found that the closest NND between $Ca_v2.1$ was 12 and 14 nm for BK and SK2, respectively. Steric hindrance likely determines the closest distance that the two particles can reside. Therefore, the random distributions were created with a constraint that no BK or SK2 location could be closer than 12 nm (BK) or 14 nm (SK2) from the location of the real $Ca_v2.1$ particles. 50 of these random distributions were created for each profile analyzed. Distributions of the real and simulated NND were compared using Kolmogorov-Smirnov test (KS-test) and judged to be significant at $p < 0.05$.

3.4.5 Analysis of spatial distance between $Ca_v2.1$ and β_4

The XY coordinates for 2nm gold particles (β_4**)** and 5 nm gold particles ($Ca_v2.1$) were plotted using iTEM software. Using a macro written in-house for the Excel software, we measured the nearest neighbor distances (NNDs) between the 2 nm gold particles and the 5 nm gold particles. Distances among $Ca_v2.1$ were measured in β_4-KO mice to see whether there is a change in $Ca_v2.1$ distribution. The XY coordinates for 5nm gold particles ($Ca_v2.1$**)** in WT and β_4-KO mice were plotted using iTEM software. Distance among $Ca_v2.1$ was then compared with those between the real $Ca_v2.1$ and the random $Ca_v2.1$ distributions. Random distributions were generated by first counting the number of $Ca_v2.1$ in each profile. Then, the same number of particles was distributed randomly within the same delineated area of the active zone. In the real distributions, we found that the closest NND among $Ca_v2.1$ was 7.9 and 7.3 nm for WT mice and β_4-KO mice, respectively. Steric hindrance likely determines the closest distance that the two particles can reside. Therefore, the random distributions were created with a constraint that no particles could be closer than 7.3 and 7.9 nm in WT mice and β_4-KO mice profile, respectively. 50 of these random distributions were created for each profile analyzed. Distributions of the real and simulated NND were compared using Kolmogorov-Smirnov test (KS-test) and judged to be significant at $p < 0.05$.

3.5 Statistical analysis

Statistical analysis was conducted with SPSS 16.0 (SPSS, Chicago). Data are presented as mean ± SD unless otherwise stated. Normal distribution was checked using Shapiro-Wilk's test. Student's t-test or ANOVA was used for data with normal distribution. For data violating normal distribution assumption we used Kruskal-Wallis test for checking significant difference. Pairwise

Mann-Whitney U test and Bonferoni correction was used if significant difference was found after Kruskal-Wallis test. Data from three animals (P3, P7, P14, P21) and four animals (P28) were pooled together when no statistical significance was detected. Correlation was checked using Spearman's rank-order test. Differences between groups were judged to be significant at $p < 0.05$.

4. Results

4.1 Sensitivity and specificity of SDS-FRL for $Ca_v2.1$ subunit

This study was conducted to accurately visualize the two-dimensional distribution of the $Ca_v2.1$ channels along the plasma membrane and to analyze channel densities quantitatively. Highly sensitive immunogold labeling in SDS-digested freeze-fracture replica (SDS-FRL) (Tanaka et al., 2005; Masugi-Tokita and Shigemoto, 2007; Lörincz and Nusser, 2010) was used in this study. As previously reported using preembedding immunogold method (Kulik et al., 2004), the presence of concentrated $Ca_v2.1$ at the presynaptic active zone of PF to PC synapses and at the postsynaptic PC spines in the perisynaptic areas was observed. A new antibody raised against an intracellular loop of $Ca_v2.1$ (Hashimoto et al., 2011; Miyazaki et al., 2012) was used for the SDS-FRL in the rat cerebellum. $Ca_v2.1$ antibody was raised in the guinea pig against 361-400 amino acid residues of mouse $Ca_v2.1$. This sequence is a part of an intracellular loop between segment I and II. As the epitope site is located at the intracellular portion of the protein, the immunogold particles for $Ca_v2.1$ were specifically distributed on the P-face in both presynaptic and postsynaptic profiles. Virtually no labeling was observed on the E-face or on the cross-fractured face. Layers of the cerebellar cortex could be easily identified in our replicas (see Fig. 3*A*) and I first evaluated the sensitivity and specificity of our replica labeling for $Ca_v2.1$ by focusing on the well-characterized presynaptic active zone of PF-PC synapses (Mintz et al., 1995; Kulik et al., 2004). This effort was performed in order to estimate the number of functional channel that can be depicted by number of gold particles for $Ca_v2.1$ in our replica sample.

The active zone of PF-PC synapses was identified (Fig. 1*A*,*B*) based on (1) the typical morphology consisting of concave shape of the P-face, higher density of intramembrane particles (IMPs) than in the surrounding areas, and dimples representing vesicle exocytosis or endocytosis

(Pfenninger et al., 1972; Hagiwara et al., 2005), and by (2) the double labeling for vesicular glutamate transporter vGluT1 (Fig. 1*A*, blue shades), which is selectively expressed in PF boutons in the molecular layer (Zander et al., 2010). While active zone of CF which can be identified with vGluT2 also showed positive labeling for $Ca_v2.1$ (Fig 2). Although vGluTs are vesicular proteins, they are often detected on presynaptic plasma membrane and thus have been used to identify the origin of presynaptic profiles (Hagiwara et al., 2005; Masugi- Tokita et al., 2007). I occasionally found small regions that were double labeled for vGluT1 and $Ca_v2.1$ that were not on a concave P-face profile but on a flat P-face profile in the molecular layer. These profiles were likely to originate from PF-interneuron synapses (Fig 3) because they lacked the concave shape and the number of PF-interneuron synapses is overwhelmed by that of PF-PC synapses (Palkovits et al., 1971; Palay and Chan- Palay, 1974). Immunogold particles for $Ca_v2.1$were concentrated in the presynaptic active zone of PF boutons as described previously (Kulik et al., 2004). These particles were not homogenously distributed throughout the active zone and small aggregations of particles were found (Fig. 1*B*, arrowheads). A recent report of the axon terminal of CA3 pyramidal cells also reveal non-homogenous distribution of immunogold particle labeled for $Ca_v2.1$ and seemingly formed small clusters (Holderith et al., 2012). At P28, the number of particles for $Ca_v2.1$ within the active zone was highly variable and ranged from 6 to 43 per active zone (Fig. 1*C*; mean = 17.1, median = 15, interquartile range = 11–21, n = 58 active zone profiles from three animals). This range was similar to that of functional $Ca_v2.1$ channel numbers deduced from calcium imaging and electrophysiological studies (14.5 to 27.3, see Discussion) indicating a high sensitivity of our SDS-FRL for $Ca_v2.1$.

The specificity of the replica labeling for $Ca_v2.1$ was confirmed using WT and $Ca_v2.1$ KO mice (Fig. 1*D*,*E*). In figure 1 D and E, I showed cross fractured sample of P-face presynaptic

site and E-face of postsynaptic site. I identified E-face of postsynaptic site with the presense of cluster of IMPs in E-face positive for glutamate receptor labeling (Masugi-Tokita and Shigemoto, 2007) in this figure I used 5 nm gold particles for AMPAR. In E-face, number of IMPs usually less than those seen in P-face, thus it was easy to identify cluster of IMPs on the background E-face with few IMPs adjacent to the cluster of IMPs. I observed a positive labeling for $Ca_v2.1$ in the adjacent P-face of presynaptic site of WT mice while in $Ca_v2.1$ KO, no labeling of $Ca_v2.1$ was found. I also found that concentrated particles for $Ca_v2.1$ in the PF presynaptic active zone in WT mice (mean = 17.7, median = 18, interquartile range = 12–21, *n* = 47 active zone from three animals) similar to those in rats but not in the KO mice (mean = 0.65, median = 0, interquartile range = 0 – 1, *n* = 31 active zone from three animals).

4.2 Distinct Patterns of $Ca_v2.1$ Distribution in PCs

4.2.1 Scattered and clustered distribution of $Ca_v2.1$

Next, I examined the distribution of $Ca_v2.1$ subunit in P28 PCs. Immunogold particles for $Ca_v2.1$ were observed throughout the soma and dendrites of PCs (Fig. 4*B*) with two distinct patterns of distribution: scattered (Fig. 4*C*, *D*) and clustered (Fig. 4*E*,*F*). The scattered pattern consists of dispersed single (isolated) particles and small aggregation of particles (3–10 particles with < 30 nm distance from the closest particle) that were found both on the P-face of soma (Fig. 4*B*, *C*) and on proximal to distal dendrites (Fig. 4*D*) of PCs. The clustered pattern of $Ca_v2.1$ immunogold particles were found within IMP clusters that were sparsely distributed on the P-face of soma and very proximal dendrites (~ 20 µm from the soma) but not distal parts of the dendrites (Fig. 3*B* shown in red, n = 7 PCs from 4 animals). The IMPs are small convex-shaped particles found in replica material and are assumed to reflect the presence of some membrane proteins. I defined IMP cluster as a group of > 10 big IMPs (diameter > 8.6 nm) with NND between each IMP shorter than 25 nm.

Virtually all of these P-face IMP clusters had concentrated particles for $Ca_v2.1$ (Fig. 4*E*, *F*), showing much larger numbers of particles within the IMP clusters than the small aggregation in the scattered pattern. The $Ca_v2.1$ immunoparticle density within the IMP clusters was 73 times higher (soma, 426.0 ± 131.3 particles/ µm^2, n = 73; proximal dendrite, 421.2 ± 163.2 particles/ µm^2, n = 40) than the density of the scattered particles (5.8 ± 1.68 particles/ µm^2, n = 4 in soma) (Fig 5). The density of the $Ca_v2.1$-labeled IMP cluster was not significantly different between soma and primary dendrite (soma, 8.1 ± 2.1 cluster/100 µm^2, n = 4, measured area 900 µm^2; primary dendrite, 8.0 ± 3.5 cluster/100 µm^2, n = 9, measured area 600 µm^2, p = 0.950, Student's t

test). Size of the $Ca_v2.1$-labeled IMP clusters was also similar between soma and primary dendrite (soma, median = 0.090 μm^2, n = 73; primary dendrite, median = 0.132 μm^2, n = 41, p = 0.93 with Mann–Whitney U test).

Specificity of the labeling for $Ca_v2.1$ in soma and dendrite was verified using wild-type and $Ca_v2.1$ KO mice. As in rats, scattered and clustered distribution patterns of $Ca_v2.1$ were found in WT mice (Fig. 3*G*, arrowheads for the scattered pattern). In $Ca_v2.1$ KO mice, no clustered immunogold particles were found (Fig. 3*H*). The density of scattered particles in $Ca_v2.1$ KO mice (0.42 ± 0.22 particles/ μm^2, n = 4 soma in 3 animals) were significantly lower than that in wild-type mice (2.3 ± 0.48 particles/ μm^2, n = 3 soma in 3 animals, p = 0.01). Interestingly, the density of the IMP cluster in soma of Cav2.1 KO mice was reduced 2.3 times compared with wild-type mice (wild-type mice, 10.3 ± 6.1 cluster/100 μm^2 , n = 9 soma in 5 animals; $Ca_v2.1$ KO mice, 4.4 ± 1.3 cluster/100 μm^2, n = 4 soma in 3 animals, p = 0.006, Mann–Whitney U test).

4.2.2 Highly variable number of $Ca_v2.1$ was found in PF and CF active zone

The role of P/Q-type calcium channel in presynaptic site is to regulate neurotransmitter release both in PF- and CF-PC synapses (Regehr and Mintz, 1994; Mintz et al., 1995; Matsushita et al., 2002). CFs which originate from inferior olivary nucleus can be differentiated from PFs since CFs innervate proximal stem dendrite of PCs (Palay and Chan-Palay, 1974), so from its location in replica sample, I could find it in the molecular layer close to the Purkinje cell layer. While PFs are granule cell axons and form more than 10^5 synapses onto distal dendrite called spinny branclets (Palay and Chan-Palay, 1974), thus I collected PF profiles in outer two-thirds of the molecular layer. Another factor to confirm CF and PF identity was to use vGluT (vesicular

glutamate transporter. The excitatory afferents to PCs, CF and PF terminals selectively express vGluT2 or vGluT1, respectively (Fremeau et al., 2001; Ichikawa et al., 2002). There was a switching from vGluT2 to vGluT1in PF terminals during developmental period (Miyazaki et al., 2003). Thus in this study, I used adult rats, which have clear separation; vGluT1 was expressed in PF while vGluT2 was expressed in CF.

In the adult rat, I compared number of $Ca_v2.1$ in PF and CF terminals. I found no difference in the number of $Ca_v2.1$ (PF, number of $Ca_v2.1$ = 15.4 ± 6.71 gold particles, cv = 0.436; CF, number of $Ca_v2.1$ = 17.4 ± 11.8 gold particles; p = 0.932 with Mann-Whitney U test, cv = 0.680; n = 45 terminals from 3 animal, Fig 6A). But the variability of $Ca_v2.1$ number in CF was larger as compare to that in PF (CF, cv = 0.68; PF, cv = 0.44). I demarcate active zone area manually along the concave shape. I found no different between active zone areas in PF and CF. The variability in density of $Ca_v2.1$ particles were larger in CF terminals compare to that in PF (PF, 0.114 ± 0.04 μm^2, cv = 0.37; PF, 0.115 ± 0.05 μm^2, cv = 0.50). These active zone areas in both terminals were correlated with the number of $Ca_v2.1$ particles (PF, r = 0.525, p = 0.000; CF, r = 0.427, p = 0.003, Spearman's rho test, Fig 6B).

4.2.3 Perisynaptic localization of $Ca_v2.1$ and co-localization with mGluR1α in PC spines.

Using the pre-embedding immunogold method, previous report showed that $Ca_v2.1$ were concentrated close to the postsynaptic density in PC spines (Kulik et al., 2004). In the present study, I verified using SDS-FRL that $Ca_v2.1$ were distributed at a high density surrounding postsynaptic membrane specialization of PF-PC synapses (Fig. 7) in paired replicas containing spines continuous with adjacent PC dendrites (Fig. 7*A,D*). A sample is separated into two parts upon freeze-fracturing and corresponding P-face and E-face profiles of the same structure can be

found in the paired replicas. Postsynaptic specialization of excitatory synapse is signified by the presence of distinct IMP clusters on the E-face (Harris and Landis, 1986). Immunogold particles for $Ca_v2.1$ were found on the P-face in areas surrounding the spine synapses (Fig. 7*C*, *F*) demarcated by the IMP cluster area projected from the corresponding E-face (Fig. 7*B*,*E*). These $Ca_v2.1$ particles were colocalized with those for metabotropic glutamate receptor mGluR1α (Fig. 7*C*, *F*), which has been also reported to be concentrated in the perisynaptic regions (Baude et al., 1993; Lujan et al., 1996) and interact directly with $Ca_v2.1$ (Kitano et al., 2003).

4.3 Density gradient of the scattered $Ca_v2.1$ along PC dendrites

Density of various ion channels in dendrites has been shown to be non-homogenous, and a gradient of the density along the proximal–distal axis has been demonstrated in pyramidal cells (Magee, 1998; Lo¨rincz et al., 2002, Lörincz and Nusser, 2010) and other types of cells (Williams and Stuart, 2000; Endo et al., 2008). It has been shown that non-homogenous distribution of channels can have a great impact on the integration of dendritic signals (Magee and Johnston, 1995; Endo et al., 2008). To evaluate whether such density gradient along PC dendrites exists for Cav2.1, I measured the density of the scattered $Ca_v2.1$ particles in primary, secondary, and distal dendrites at P28. The primary dendrite was identified as the dendrite continuum with the soma before the first major division (Fig. 4). Dendrites with diameter larger than 2 µm found in the proximal half of the molecular layer were defined as secondary dendrites and dendrites with diameter smaller than 2µm found in the distal half of the molecular layer were defined as distal dendrites. Graded increase in the density of the scattered $Ca_v2.1$ particles was found from the soma to the distal dendrites (Fig. 8*A*). Distal dendrites had 2.5 times higher

density of scattered $Ca_v2.1$ particles than soma and primary dendrites (Fig. 8*A*; $p = 0.001$ for soma vs distal dendrites; $p = 0.003$ for primary vs distal dendrites, Kruskal–Wallis test, pairwise Mann–Whitney *U* test, and Bonferroni correction). As described in a previous section (Fig. 4), scattered $Ca_v2.1$ particles can be subdivided into isolated particles and particles forming small aggregations. The density of isolated $Ca_v2.1$ particles in distal dendrites was also significantly higher than that in soma (Fig. 8*B*; $p = 0.004$, Kruskal–Wallis test, pairwise Mann–Whitney *U* test, and Bonferroni correction). The density of the small aggregation was also 2.7 times higher in distal dendrites than in soma (Fig. 8*C*, $p = 0.003$, Kruskal–Wallis test, pairwise Mann–Whitney *U* test, and Bonferroni correction).

4.4 Development of scattered and clustered $Ca_v2.1$ distributions

Next, developmental change in $Ca_v2.1$ distribution was examined. First, the density of the scattered $Ca_v2.1$ immunogold particles at the soma, including both the isolated particles and particles forming small aggregations, from P3 to adult was compared (Fig. 9D). The density of the scattered $Ca_v2.1$ particles was low at P3 and P7 but the density significantly increased at the second postnatal week (p = 0.007 for P3 vs P14, p = 0.01 for P7 vs P14, ANOVA and Tukey's test). The scattered particle density remained constant at later ages. When I compared the density of the scattered $Ca_v2.1$ particles with the density of the clustered particles within each P-face IMP cluster, I found a relative increase in the density of the scattered particles with development (ratios of scattered particle density over clustered particle density, P3 = 0.0057, P7 = 0.0035, P14 = 0.0091, P28 = 0.014, adult = 0.030).

Next, development of the clustered distribution pattern of $Ca_v2.1$ was examined. I observed such clustered distribution in soma at all ages examined (Fig. 9*A–D*). The size of $Ca_v2.1$-labeled IMP clusters (Fig. 9*E*) significantly increased from P7 to P14 (p = 0.000), remained constant until P28, but increased again in the adult (p = 0.000 for adult vs P7, P14, P21, and P28, Kruskal–Wallis test, pairwise Mann–Whitney*U*test, and Bonferroni correction). The number of immunogold particles within each IMP cluster (Fig. 9*F*) significantly increased from P7 to P28 (p = 0.000, Kruskal–Wallis test, pairwise Mann–Whitney U test, and Bonferroni correction) but decreased in adult (p = 0.001 for adult and P21; p = 0.031 for adult and P28 Kruskal–Wallis test, pairwise Mann–Whitney U test, and Bonferroni correction). The density of $Ca_v2.1$ particles in IMP clusters was similar among P7, P14, and P28 (426 to 474 particles/μm^2), slightly higher in P21 (499 particles/ μm^2), but significantly decreased in adult (175

particles/μm^2, p = 0.000, for adult vs P7, P14, P21, P28, Kruskal–Wallis test, pairwise Mann–Whitney U test, and Bonferroni correction). At all ages, the IMP cluster size and the particle number showed a strong positive correlation (Fig. 9*G*; r = 0.84, 0.91, 0.94, 0.91, 0.51 for P7, P14, P21, P28, and adult, respectively, p = 0.000 for each age, Spearman's rank-order test, n = 62–73). I also examined the density of the Cav2.1-labeled IMP clusters at the soma and found a significant increase from P3 and P7 to P28 and adult (Fig. 9*H*; p = 0.05 for P3 and 7 vs P28 and adult, total measured area 500–1000 μm^2). These results demonstrate that the $Ca_v2.1$-labeled IMP clusters at the PC ~~cell~~ body develop rapidly at around the second postnatal week with an additional developmental change continuing even after the fourth postnatal week.

$Ca_v2.1$ particles appeared not to be evenly distributed throughout the IMP cluster area (Fig. 9). To examine whether these particles are randomly distributed or clustered within the IMP cluster area, the NNDs between each immunogold particle were measured and the distribution of these NNDs was compared with that of randomly distributed NNDs that were generated with the same particle numbers and IMP cluster areas. I found that the distribution of the real NNDs was significantly different from that of the random NNDs (p < 0.01 Kolmogorov– Smirnov test) and the real NNDs had a smaller median value (real, median = 23.5 nm, n = 719; random, median = 24.1 nm, n = 1292, p = 0.03, Mann–Whitney U test). This indicates the presence of tight clustering of $Ca_v2.1$ within the IMP cluster, which is likely to be actively regulated.

4.5 Co-localization of $Ca_v2.1$ with calcium-activated potassium channels within the calcium nanodomain

Previous studies show that a subtype of calcium-activated potassium channel (KCa), BK channel, also has two distinct types of localization, a scattered pattern and a clustered pattern, at the somatic plasma membrane of PCs and pyramidal cells (Kaufmann et al., 2009, 2010). Electrophysiological experiments demonstrate that the activation of BK as well as another KCa, SK2 channels, is regulated by calcium influx through P/Q-type VDCCs (Womack et al., 2004). To understand the spatial relationship between $Ca_v2.1$ and BK and SK2 channels, co-localization of the channels were examined by double labeling with 5 and 10 nm immunogold particles (Fig. 10). First, using single labeling, immunogold particles for BK or SK2 channels were found concentrated in the P-face IMP clusters at PC soma (Fig. 10 *A*, *B*). Such distribution looked very similar to the clustered distribution pattern of the Cav2.1. Double immunogold labeling revealed striking co-localization of $Ca_v2.1$ with BK or SK2 channels in these IMP clusters (Fig. 10 *C*,*D*). It should be noted that application of two different primary antibodies in double labeling experiment could lead to false negative results due to the interference between the two antibodies that results in a decreased labeling efficiency. To minimize the underestimation of co-localization, I applied the two antibodies sequentially with reversed orders in the double labeling experiments (Kasugai et al., 2010). I found virtually 100% co-localization of $Ca_v2.1$ with either BK or SK2 channels in the IMP cluster area (Table 1). Conversely, no noticeable co-localization of the scattered $Ca_v2.1$ with either of BK or SK2 channels was observed in PC, although particles for BK and SK2 also showed scattered distribution in soma, dendrites, and spines (data not

shown). The co-localization with the K_{Ca} particles was not observed even for the small aggregation of $Ca_v2.1$ particles.

I confirmed the specificity of our BK and SK2 labeling using replica species from BK and SK2 KO mice (Fig. 10 *E*, *F*). Immunogold particles for BK or SK2 channels were mostly abolished in the respective KO mice (BK KO, 0.25 ± 0.12 particles/μm^2,WT mice, 5.24 ± 1.80 particles/ μm^2; SK2 KO, 0.069 ± 0.056 particles/ μm^2,WT mice, 2.41 ± 0.53 particles/ μm^2), but those for $Ca_v2.1$ remained. The density of IMP clusters found in BK and SK2 KO soma was also reduced to half compared with those in wild-type mice (wild-type mice, 10.3 ± 6.1 cluster/100 μm^2 n = 9 soma in 5 animals; BK KO mice, 4.5 ± 1.0 cluster/100 μm^2 n = 4 soma in 3 animals, p = 0.003 vs wild-type; SK2 KOmice, 4.8 ± 2.3 cluster/100 μm^2, n = 5 soma in 3 animals, p = 0.019 vs wild-type, Mann–Whitney *U* test).

As the $[Ca^{2+}]i$ rapidly decreases with increase in distance from the calcium influx source, the distance between $Ca_v2.1$ and K_{Ca} would likely determine the efficacy of K_{Ca} activation following $Ca_v2.1$ activation. To examine the extent of the spatial coupling between these channels, the NNDs between immunogold particles for $Ca_v2.1$ (5 nm) with immunogold particles for BK or SK2 (10 nm) were measured in our double-labeled replicas at P28. The median of the NNDs between $Ca_v2.1$ and either BK or SK2 particles were 37.8 nm (interquartile range, 27.3–60.3 nm) and 38.9 nm (interquartile range, 29.9–49.5 nm), respectively. Although these median values were not significantly different (p = 0.69, Mann–Whitney *U* test), distributions of these two kinds of NNDs showed significant difference (p = 0.019 for Kolmogorov–Smirnov test). To examine specific spatial association of $Ca_v2.1$ with BK or SK2 channels, random distributions for BK and SK2 particles were generated within the IMP cluster areas and the NNDs between these particles and the real $Ca_v2.1$ particles were measured. I found significantly smaller NNDs

for the real SK2 and Cav2.1 particles (median, 38.9 nm) than or the randomly distributed SK2 particles (median, 43.9 nm $p < 0.05$, Mann–Whitney *U* test, $p = 0.001$, Kolmogorov–Smirnov test, Fig. 9*B*), whereas no significant difference was detected between the real and random NNDs for BK toward $Ca_v2.1$ (Fig. 11*A*). This result suggests that SK2 but not BK channels are specifically targeted to have close association with $Ca_v2.1$ channels. However, as these three channels do colocalize within the same IMP cluster areas, the distance between $Ca_v2.1$ and BK or SK2 channels is already very close. Thus, both types of KCa are likely to be within the calcium nanodomain created by the $Ca_v2.1$ activation at the soma and proximal dendrites of PCs.

4.6 Co-localization of $Ca_v2.1$ with β_4 subunit within PF active zone

I would like to answer the question whether special arrangement of $Ca_v2.1$ in the active zone has something to do with the interaction of $Ca_v2.1$ (α_1A subunit) and β subunit. As it is reported previously, β_4 subunit is the predominant subunit associated with the P/Q-type calcium channels. The overall expression pattern and cellular localization in in situ hybridization data, suggested that β_4 may associate predominantly but probably not exclusively with the α_1A subunit in the cerebellum since moderate expression of β_3 was also seen (Ludwig et al., 2003).

Since β subunit is entirely cytosolic, I used different fracturing and SDS digestion method with previous samples. Instead of coating with carbon, platinum carbon and final application of carbon layer, I used only carbon layer in order to enhance labeling intensity and visualization of 2 nm particles. Shorter time in SDS digestion period would allow higher retention of β subunit in replica. In this carbon replica, I use 2nm gold particles for β_4 labeling. Immunogold particles for β_4 were concentrated in the presynaptic active zone of PF boutons. These particles were not homogenously distributed throughout the active zone and small aggregations of particles were found (Fig. 12*B*, white arrowheads). The labeling of β_4 was mostly abolished in β_4-KO mice. Double labeling of β_4 and $Ca_v2.1$ in β_4-KO mice showed only $Ca_v2.1$ labeling.

Next I performed $Ca_v2.1$ labeling in β_4-KO mice to examine whether there is a change in $Ca_v2.1$ number and density in PF active zone as compare with WT mice. No significant difference was found in the number and density of $Ca_v2.1$ (β_4-KO mice, 18.9 ± 8.37 gold particles, density = 144± 46.6 gold particles/μm^2; WT mice, 24.2 ± 12.5 gold particles, density = 188 ± 78.6 gold particles/μm^2, Mann Whitney U test). The real NNDs had smaller median values as compared with random NNDs in WT and β_4-KO (WT mice, real, median = 23.4 nm, n = 317; random, median = 37 nm, n = 11959, p = 0.00, Mann–Whitney U test; β_4-KO mice, real, median

= 23.2 nm, *n* = 433; random, median = 39.2 nm, *n* = 13138, *p* = 0.000, Mann–Whitney *U* test). The distribution of the NNDs was significantly different from that of the random NNDs simulated with the same number and density of particles in WT and β_4-KO (*p* = 0.000 Kolmogorov– Smirnov test). This indicates that the clustering of $Ca_v2.1$ in PF active zone was not disturbed in β_4-KO mice. Thus the presence or absence of β_4 does not interfere with spatial arrangement of $Ca_v2.1$ particles in PF active zone.

The β subunits interact with α_1 subunits through the direct interaction. Thus I first examined the colocalization of these two molecules in our replica samples. In double labeled samples from adult rats, I measured NNDs from 5 nm gold particles (α_1A subunit) towards 2 nm gold particles (β_4 subunit). I found that the median of NNDs between $Ca_v2.1$ and β_4 were 215 nm (interquartile range, 100.5 – 295 nm, Figure 13).

5. Discussion

5. DISCUSSION

5.1 General

This study provides the two-dimensional distribution of VDCCs along the plasma membrane using highly sensitive SDS-FRL. Due to the lack of decent antibodies, only a few previous studies have described the VDCC distribution using conventional preembedding immunogold methods (Hanson and Smith, 2002; Kulik et al., 2004; Parajuli et al., 2010). Knowing the precise localization of the channel at nano-scale resolution is of especial value for the VDCCs as the calcium signal created by these channels is often restricted to the nanodomain and thus the VDCCs are likely to be carefully arranged to serve finely-tuned cellular functions. Among the various VDCCs, $Ca_v2.1$ is of particular importance in cerebellar functions. I confirmed the $Ca_v2.1$ localization in the presynaptic active zone of PF- and CF-PC synapses which has high variable number of $Ca_v2.1$ gold particles, and $Ca_v2.1$ gold particles were arranged not homogenously distributed inside the active zone of both terminals. In postsynaptic compartment, I confirmed perisynaptic localization of $Ca_v2.1$ gold particles at the edge of PSD in spine. I further discovered two distinct patterns of Cav2.1 distribution in PCs, the scattered and the clustered patterns. The scattered $Ca_v2.1$ is distributed non-uniformly from soma to distal dendrite with graded increase in its density. The clustered $Ca_v2.1$ is concentrated within IMP clusters on PC soma and proximal dendrites, and colocalized with two types of KCa, BK, and SK2, making calcium nanodomains. These two distinct types of localization are developmentally regulated, becoming mostly mature in the second postnatal week. I also revealed that the β_4 subunit was colocalized with $Ca_v2.1$ inside the active zone of PF terminals. However, I couldn't detect any

difference in number, density, spatial arrangement of $Ca_v2.1$ gold particles inside PF active zone in the absence of β_4.

5.2 The number and the labeling efficiency of $Ca_v2.1$ channels in presynaptic active zone

Although recording of any cellular activity at the small presynaptic terminal is often demanding with either electrophysiological or imaging techniques, several reports provided indirect clues that enabled us to estimate the number of functional $Ca_v2.1$ in PF presynaptic active zones. I used these estimates to assess the labeling efficiency of $Ca_v2.1$ with our SDS-FRL. By using two-photon calcium concentration imaging, Brenowitz and Regehr (2007) estimated that the number of calcium ions entering a PF bouton upon presynaptic action potential firing is 11,000 on average. Therefore, the charge influx via calcium channels should be twice from the charge of an electron. A single PF bouton has 1.05–1.12 active zones on average in young rodents (Napper and Harvey, 1988; Kurihara et al., 1997). Using serial ultrathin sections, I found 1.09 synapses per single PF bouton on average in P17 rat (n = 145 boutons from 2 animals, data not shown). The calculated charge influx should be divided by this number to obtain the charge influx per active zone. $Ca_v2.1$ channels mediate 50% of the calcium concentration increase with presynaptic action potential at P9–P14 (Mintz et al., 1995). Therefore, charge influx through $Ca_v2.1$ channels is calculated as 1.62 fC.

The ensemble average of the expected charge carried by a single calcium channel in response to a presynaptic action potential can be calculated as follows. Bischofberger et al. (2002) measured the total calcium influx in a mossy fiber bouton as 119 fC on average by direct presynaptic recording. Using nonstationary fluctuation analysis of the calcium current in the same preparation, Li et al. (2007) estimated that the total number of calcium channels present is

2007 on average. These results indicate that 59.3 aC is the expected charge carried by a single calcium channel. Another estimate of the expected charge influx through single calcium channel can be obtained by using the gating model of the P/Q-type calcium channel (Li et al., 2007), and it was calculated as 112 aC (P. Jonas, personal communication). If I divide the total $Ca_v2.1$ channel-mediated charge influx per PF active zone (1.62 fC), with the expected charge influx through single channels, I obtain 14.5–27.3 as the expected number of functional P/Q-type channels present. Our SDS-FRL showed 17.1 $Ca_v2.1$ particles on average in a single PF active zone, giving the estimated labeling efficiency of 62.6–118%. Although these are approximate estimates, the sensitivity of our SDS-FRL for $Ca_v2.1$ was expected to be very high and likely to be similar to that for functional AMPA receptors, which was close to unity (Tanaka et al., 2005). Brenowitz and Regehr (2007) found heterogeneity in the amplitude of presynaptic calcium transients in response to single action potentials among PF boutons (CV = ~0.40). This is consistent with our results showing a large variability of $Ca_v2.1$ particles per active zone (6 to 43, CV = 0.47). The size of the PF-PC synapse was similarly variable ranging from 0.04 to 0.36 μm^2 (0.15 ± 0.08 μm^2, CV = 0.53) (Harris and Stevens, 1988). Since a positive correlation was found between the number of $Ca_v2.1$ and the area of presynaptic active zone, the variability of the total $Ca_v2.1$ number is at least partly ascribable to the variability of the synapse size.

5.3 High number of $Ca_v2.1$ scales with area of active zone in PF and CF terminals

PCs receive two different kinds of excitatory synaptic inputs. The first one originates from inferior olive, known as CF and later originates from cerebellar granule cells that send their axons into the cerebellar molecular layer as PF (Palay and Chan-Palay, 1974). These two inputs exhibit differences in short-term plasticity and initial probability of release. It is of general

interest to examine the two synapses which have different properties while synapsing onto the same target neurons. One approach to seek the answer for the different between them has been to compare their anatomical structures. The hypothesis that derived from the basis of probability of release is that it is proportional to the number of docked vesicles. However previous study by Xu-Friedman et al., 2001 found that both PF and CF have same number of anatomically docked vesicles, same active zone area (as measured in PSD size) with high variability in CF compare to PF. Thus difference in probability of release does not correlate with difference in number of docked vesicles at these synapses. My study agrees well with the data that there was high variability in active zone area of CF compare to PF and number of docked vesicles at both synapses was correlated well with the active zone area (Xu-Friedman et al., 2001).

High variability in the number $Ca_v2.1$ particles correlates with high variability in active zone area. The numbers of several active-zone proteins, including presynaptic calcium channels, scale linearly with the active-zone area (Holderith et al., 2012). However this high variability in active zone area, numbers of active proteins (such as calcium channels) didn't correlate with different in the release probability and short-term plasticity between CF and PF synapses.

5.4 Perisynaptic localization of $Ca_v2.1$ and its colocalization with mGluR1 in PC spines

The dendritic localization of $Ca_v2.1$ has a role in generating dendritic calcium transients upon depolarization. With electrophysiological method, generation of dendritic calcium transients is partially due to the calcium influx through VDCCs which is probably $Ca_v2.1$ as the abundant calcium channel found in PCs (Konnerth et al., 1992). This study is in agreement with previous study using preembedding method, that $Ca_v2.1$ was located with the highest density at sites of the extrasynaptic membrane between 0-180nm away from PSD (Kulik et al., 2002). Other

glutamate receptor that also has been found to be located in the extrasynaptic site of PC spines is mGluR1α (Luján et al., 1997) which also observed with SDS-FRL method (Figure 7C and F, 10 nm gold particles). With immunohistochemistry method, colocalization of $Ca_v2.1$ and mGluR1α was also seen in the molecular layer of the cerebellum where PC dendrites and spines are located (Kitano et al., 2003). Both $Ca_v2.1$ and mGluR1α can activate inositol-1,4,5-triphosphate (IP_3) production, through depolarization-induced Ca^{2+} influx then activation of AMPA receptors and later by direct mGluR1α activation (Okubo et al., 2001). This synergistic activation of IP_3 by $Ca_v2.1$ and mGluR1α can ensures spatiotemporal regulation of $[Ca^{2+}]_i$ in glutamatergic neurotransmission (Kitano et al., 2003).

5.5 Functional role of the $Ca_v2.1$ gradient along PC dendrite and its development

VDCCs localized to the PC dendrites induce dendritic spikes after CF activation (Llinás and Sugimori, 1980) or strong PF activation (Llina´s and Nicholson, 1971). Dendritic spikes were shown to be initiated at 10–25 µm from the PC soma (Pouille et al., 2000). The disappearance of clustered $Ca_v2.1$ coincides with this location of dendritic spike initiation, which suggests that the scattered rather than the clustered $Ca_v2.1$ channels take part in the dendritic spike initiation and its propagation. Previous calcium imaging studies showed larger increases of $[Ca^{2+}]$i during bursts of calcium spikes in the thinner dendrites of PCs (Ross et al., 1990; Lev-Ram et al., 1992). The difference in the surface-to-volume ratio and/or the difference in the VDCC density could explain such phenomenon. Our results indicate that the density gradient of the scattered $Ca_v2.1$ contributes to the difference in $[Ca^{2+}]$i signals in the distal and proximal dendrites. Gradient increase of VDCC density from soma to dendrites has been described for L-type channels in globus pallidus neurons (Hanson and Smith, 2002) and low-voltage-activated calcium channels

in deep cerebellar nuclei neurons (Gauck et al., 2001). Such gradient as well as the preferential positioning of VDCCs in perisynaptic sites as found in our studies could have a role in amplifying and modifying synaptic signals (Hanson and Smith, 2002). Developmental change of the non-homogenous distribution of $Ca_v2.1$ along the dendrite could also have a role in the emergence of trimodal pattern activity upon maturation of the cerebellum (Womack and Khodakhah, 2002). Increases in the area of the IMP clusters, the number of $Ca_v2.1$ within the clusters, and the density of the scattered $Ca_v2.1$ were found to occur from the first to second postnatal week. Previous studies reported that $Ca_v2.1$ in PCs is essential for homosynaptic competition among multiple CFs (Miyazaki et al., 2004), competition between CF and PF (Miyazaki et al., 2012), and refining process at early phase (around P12) of CF synapse elimination (Hashimoto et al., 2011). The developmental change of $Ca_v2.1$ distribution after the first postnatal week is likely to take a role in such maturation process of the cerebellar circuit.

5.6 Calcium nanodomain in PC soma and proximal dendrites

Based on electrophysiological experiments using exogenous calcium chelators, EGTA and BAPTA, local calcium signaling domain was classified into: (1) “calcium nanodomain” (~20–50 nm from the calcium source) that is effectively interfered by BAPTA but not EGTA, and (2) “calcium microdomain” (50 nm to a few hundred nanometers from the calcium source) that is sensitive to both BAPTA and EGTA (Neher, 1998). In the present study, two types of KCa, BK and SK2, were found to colocalize with $Ca_v2.1$ in the nanodomain range (~40 nm NND) within P-face IMP clusters. It has been reported that the outward current mediated by BK is strong enough to counteract the inward current delivered by the activation of $Ca_v2.1$ during dendritic spikes and contributes to afterhyperpolarization in PCs (Raman and Bean, 1999; Rancz and

Häusser, 2010). Direct interaction of $Ca_v2.1$ and BK proteins was also found by copurification of these two molecules from rat brain in tandem mass spectrometry (Berkefeld et al., 2006). On the other hand, activation of SK2 has been reported to control the firing frequency of PCs (Edgerton and Reinhart, 2003). These two KCa differ in their affinity to calcium with BK having lower affinity (3 – 50 µM) (Womack and Khodakhah, 2002) than the SK2 (300 nM, Bond et al., 1999). Furthermore, I found closer association of SK2 than BK in their spatial relationship to the $Ca_v2.1$. More instant interaction of SK2 than BK with $Ca_v2.1$ in the same nanodomain can contribute to the precise regulation of firing frequency of PCs. In episodic ataxia 2 (EA2) model mice, reduced activation of SK channels associated with a decrease in the P/Q-type calcium current (Barclay et al., 2001) caused decreases in the precision of PC pacemaking (Walter et al., 2006). Furthermore, pharmacological increase of SK channel activity recovered not only the pacemaking but also ataxia. In BK KO mice, reduced spontaneous activity of PCs due to depolarization-induced inactivation of action potential mechanism was associated with cerebellar ataxia (Sausbier et al., 2004). The nanodomain formed with $Ca_v2.1$ and these two KCa channels may thus contribute to cerebellar coordination through different mechanisms. The P-face IMP clusters in PC soma have been shown to overlay subsurface cisterns (Henkart et al., 1976; Kaufmann et al., 2009), which are enriched with IP_3R and ryanodine receptor (RyR) known as plasmerosomes (Walton et al., 1991; Blaustein and Golovina, 2001). Reduced density of IMP clusters on Purkinje cell bodies in KO mice of $Ca_v2.1$, BK, and SK2 suggests that interactions between these molecules may contribute to the formation of the plasmerosomes. Junctophilins, a family of junctional membrane complex protein, have been shown to contribute to the formation of complex between endoplasmic/sarcoplasmic reticulum and plasma membranes in cardiac myocytes (Takeshima et al., 2000) and support Ca^{2+}-mediated communication between RyR and

SK2 (Kakizawa et al., 2007). It is possible that from my study newly found calcium nanodomain formed by $Ca_v2.1$, BK, and SK2 is functionally coupled to IP_3R and RyR on the subsurface cistern as well, and the intricate interactions among these channels could fine-tune PC excitability.

5.7 β_4 is the β-subunit partner of $Ca_v2.1$ in PF terminal

It is important to find out which β subunits are associated with $Ca_v2.1$, since β subunits can regulate the assembly and membrane localization of α_1 subunit (Nishimura et al., 1993; Chien et al., 1995). In the cerebellum, high expression of β_4 and moderate expression of β_3 subunit were reported at mRNA (Ludwig et al., 1997) and protein levels (Ferrándiz-Huertas et al., 2012). The β_4 subunit is expressed throughout developmental ages with increasing levels in mature age suggesting that this subunit is important in the developing cerebellum (Vance et al., 1998; Ferrándiz-Huertas et al., 2012). Expression of β_3 subunits was decreased after the second postnatal week (Ferrándiz-Huertas et al., 2012). Thus in this study, I examined expression of β_4 subunits in adult rat cerebellum.

In this study, there were no differences in number and density of $Ca_v2.1$ gold particles between WT and β_4 KO mice. This result is in agreement with a previous study on lethargic brain, showing immunolocalization of $Ca_v2.1$ indistinguishable from wild type mice (Billings et al., 2012). Furthermore, in dissociated lethargic PC neurons, large amplitude of P-currents was observed, showing that electrophysiological properties of $Ca_v2.1$ are not regulated by β_4 subunit may be rescued by $\beta_{1\text{-}3}$ subunit reshuffling (Burgess et al., 1999). So in this study, β_4 subunit was not essential for expression and clustering of $Ca_v2.1$.

A previous study found that β_4 subunit is colocalized with ELKS1 (CAST2) in the molecular layer of the cerebellum (Billings et al., 2012). Localization of β_4 subunits in $Ca_v2.1$-KO mice was found to be disrupted confirming interaction between these two molecules in vitro (Billings et al., 2012). A pull-down assay revealed that the β_4 subunit interacted directly with at least N- and C-terminal regions of CAST. Co-expression of CAST and $Ca_v2.1$ in baby hamster kidney (BHK) cells caused a change in voltage dependence shifting toward the hyperpolarizing direction (Kiyonaka et al., 2012). Thus it is possible that interaction between $Ca_v2.1$, β_4 subunit, and ELKS1 may regulate neurotransmitter release in the presynaptic active zone.

5.8 Conclusion

In conclusion, I confirm the efficiency of our SDS-FRL method, 62.6–118% as compared to number of functional $Ca_v2.1$ by electrophysiological method. $Ca_v2.1$ was found in the active zone of PF and CF terminals with special arrangement and not homogenously distributed, showing that these arrangements are actively regulated. In postsynaptic site, location of $Ca_v2.1$ in perisynaptic site from PSD and colocalized with mGluR1α can have an impact in ensuring spatiotemporal $[Ca^{2+}]_i$ in PC neurotransmission. While in somatodendritic compartment, there are two distinct distribution patterns of $Ca_v2.1$ found in PCs, scattered and clustered distribution. Both populations of $Ca_v2.1$ were already seen at P3, first postnatal week of rat's life which is critical time in synapse arrangement during development of cerebellum. In PC soma, both populations were increased in density from the second postnatal week until adulthood, suggesting there is developmental changes in $Ca_v2.1$ until it become the most abundant calcium channel found in cerebellum. In addition, I showed that the difference in $[Ca^{2+}]_i$ between thinner and thicker dendrites from previous calcium imaging studies can be due to higher density of

$Ca_v2.1$ found in distal dendrite (thinner dendrite) as compare to soma and proximal dendrite (thicker dendrites). Other population of $Ca_v2.1$ which has 74-fold higher densities compare to scattered distribution, clustered distribution, was found within the clusters of IMP found in P-face of soma and proximal dendrite. I found that virtually all of the $Ca_v2.1$ clusters were co-localized with two types of calcium-activated potassium channel, BK and SK2 channel with the nearest neighbor distance ~40nm. The arrangement of calcium nanodomain created by opening of $Ca_v2.1$ channels likely activates the two potassium channels that limit the extent of depolarization. Furthermore, I found that β subunit partner for $Ca_v2.1$ in the active zone of PF presynaptic site was β_4. However, β_4 subunit was not essential for expression and clustering of $Ca_v2.1$ in the presynaptic active zone.

ACKNOWLEDGEMENTS

I would like to thank Dr. Naomi Kamasawa for her endless effort and time teach me how to conduct SDS-FRL experiment. I learned a lot from her how to differentiate each compartment of cerebellum in this replica sample. She also taught me how to analyze and represent my data so that it will help other people understand the message behind each picture that I showed from this technique. It was such a nice experience to learn from an expert like her.

I would like to thank Prof. Dr. Ryuichi Shigemoto for allowing me to stay in his lab thought all this 5 years-Phd time. I felt grateful also since under his supervision he allowed me to study all technique that will be useful for my studies and always believe in me every time I face failure in my experiment. It really had been a great supporter academically for me.

I appreciate Dr. Yugo Fukazawa and Dr. Ko Matsui for their educating, caring and always giving problem solving every time I had a problem with my experiment. I also want to thank all of lab members and friends for always helping me and being a nice supporter for me. Their presence means everything for me to make my life less burden here in Japan.

Many thank to SOKENDAI and NIPS for giving me such comfortable environment for my studies. And I would like to thank the doctoral thesis committee: Prof. Dr. R. Shigemoto, Prof. Dr. Y. Kawaguchi, Prof. Dr. Y. Yoshimura, Prof. M. Fukata and Prof. Dr. M. Watanabe, for their time to evaluate my thesis.

Lastly I want to thank the Director of my life, my twin sister, my husband, my parent, beautiful little me, my sister and all my relatives for their love and support during my PhD years.

REFERENCES

Akita T, Kuba K (2000) Functional triads consisting of ryanodine receptors, Ca^{2+} channels, and Ca^{2+}-activated K^+ channels in bullfrog sympathetic neurons. J Gen Physiol 116:697–720.

Barclay J, Balaguero N, Mione M, Ackerman SL, Letts VA, Brodbeck J, Canti C, Meir A, Page KM, Kusumi K, Perez-Reyes E, Lander ES, Frankel WN, Gardiner RM, Dolphin AC, Rees M (2001) Ducky mouse phenotype of epilepsy and ataxia is associated with mutations in the *Cacna2d2* gene and decreased calcium channel current in cerebellar Purkinje cells. J Neurosci 21:6095– 6104.

Baude A, Nusser Z, Roberts JD, Mulvihill E, McIlhinney RA, Somogyi P (1993) The metabotropic glutamate receptor (mGluR1α) is concentrated at perisynaptic membrane of neuronal subpopulations as detected by immunogold reaction. Neuron 11:771–787.

Berkefeld H, Sailer CA, Bildl W, Rohde V, Thumfart JO, Eble S, Klugbauer N, Reisinger E, Bischofberger J, Oliver D, Knaus HG, Schulte U, Fakler B (2006) BKca-Cav channel complexes mediate rapid and localized Ca^{2+}-activated K^+ signaling. Science 314:615– 620.

Berridge MJ (2002) The endoplasmic reticulum: a multifunctional signaling organelle. Cell Calcium 32: 235–249.

Bichet D, Cornet V, Geib S, Carlier E, Volsen S, Hoshi T, Mori Y, De Waard M (2000) The I-II loop of the Ca^{2+} channel alpha 1 subunit contains an endoplasmic reticulum retention signal antagonized by the beta subunit. Neuron 25:177-190.

Bischofberger J, Geiger JR, Jonas P (2002) Timing and efficacy of Ca^{2+} channel activation in hippocampal mossy fiber boutons. J Neurosci 22:10593–10602.

Billings SE, Clarke GL, Nishimune H (2012) ELKS1 and Ca^{2+} channel subunit β_4 interact and colocalize at cerebellar synapses. Neuroreport 23(1): 49-54.

Blaustein MP, Golovina VA (2001) Structural complexity and functional diversity of endoplasmic reticulum Ca^{2+} stores. Trends Neurosci 24:602– 608.

Bond CT, Maylie J, Adelman JP (1999) Small-conductance calciumactivated potassium channels. Ann NY Acad Sci 868:370 –378.

Brenowitz SD, Regehr WG (2007) Reliability and heterogeneity of calcium signaling at single presynaptic boutons of cerebellar granule cells. J Neurosci 27:7888 –7898.

Burgess DL, Biddlecome GH, McDonough SI, Diaz ME, Zilinski CA, Bean BP, Campbell KP, Noebels JL (1999) Beta subunit reshuffling modifies N- and P/Q-type Ca^{2+} channel subunit compositions in lethargic mouse brain. Mol Cell Neurosci 13:293-311.

Chien AJ, Zhao X, Shirokov RE, Puri TS, Chang CF, Sun D, Rios E, Hosey MM (1995) Roles of a membrane-localized β subunit in the formation and targeting of functional L-type Ca^{2+} channels. J Biol Chem 270: 30036-30044.

Cueni L, Canepari M, Luja´n R, Emmenegger Y, Watanabe M, Bond CT, Franken P, Adelman JP, Lu¨thi A (2008) T-type Ca^{2+} channels, SK2 channels and SERCAs gate sleep-related oscillations in thalamic dendrites. Nat Neurosci 11:683– 692.

Davie JT, Clark BA, Ha¨usser M (2008) The origin of the complex spike in cerebellar Purkinje cells. J Neurosci 28:7599 –7609.

De Schutter E, Bower JM (1994) Simulated responses of cerebellar Purkinje cells are independent of the dendritic location of granule cell synaptic inputs. Proc Natl Acad Sci U S A 91:4736–4740.

De Waard M, Pragnell M, Campbell KP (1994) Ca^{2+} channel regulation by a conserved beta subunit domain. Neuron 13:495-503.

Edgerton JR, Reinhart PH (2003) Distinct contributions of small and large conductance Ca^{2+}-activated K^{+} channels to rat Purkinje neuron function. J Physiol 548:53– 69.

Endo T, Tarusawa E, Notomi T, Kaneda K, Hirabayashi M, Shigemoto R, Isa T (2008) Dendritic Ih ensures high-fidelity dendritic spike responses of motion-sensitive neurons in rat superior colliculus. J Neurophysiol 99: 2066–2076.

Ferrándiz-Huertas C, Gil-Mínquez M, Luján R (2012) Regional expression and subcellular localization of the voltage-gated calcium channel β subunits in the developing mouse brain. J Neurochem 22 (6): 1095-107.

Fremeau, RT. Jr, Troyer MD, Pahner I, Nygaard GO, Tran CH, Reimer RJ, Bellocchio EE, Fortin D, Storm-Mathisen J, Edwards RH (2001) The expression of vesicular glutamate transporters defines two classes of excitatory synapse. Neuron 31: 247-260.

Fujimoto K (1995) Freeze-fracture replica electron microscopy combined with SDS digesstion for cytochemical labeling for integral membrane proteins. Application to the immunogold labeling of intercellular junctional complexes. J Cell Sci 108:3443–3449.

Fujita A, Cheng J, Hirakawa M, Furukawa K, Kusunoki S, Fujimoto T (2007) Gangliosides GM1 and GM3 in the living cell membrane form clusters susceptible to cholesterol depletion and chilling. Mol Biol Cell 8(6): 2112-2122.

Gauck V, Thomann M, Jaeger D, Borst A (2001) Spatial distribution of low and high-voltage-activated calcium currents in neurons of the deep cerebellar nuclei. J Neurosci 21:RC158.

Hagiwara A, Fukazawa Y, Deguchi-Tawarada M, Ohtsuka T, Shigemoto R (2005) Differential distribution of release-related proteins in the hippocampal Ca3 area as revealed by freeze-fracture replica labeling. J Comp Neurol 489:195–216.

Hanson JE, Smith Y (2002) Subcellular distribution of high-voltage activated calcium channel subtypes in rat globus pallidus neurons. J Comp Neurol 442:89 –98.

Harris KM, LandisDM (1986) Membrane structure at synaptic junctions in area CA1 of the rat hippocampus. Neuroscience 19:857– 872.

Harris KM, Stevens JK (1988) Dendritic spines of rat cerebellar Purkinje cells: serial electron microscopy with reference to their biophysical characteristics. J Neurosci 8:4455– 4469.

Hashimoto K, Tsujita M, Miyazaki T, Kitamura K, Yamazaki M, Shin HS, Watanabe M, Sakimura K, Kano M (2011) Postynaptic P/Q-type Ca^{2+} channel in Purkinje cell mediates synaptic competition and elimination in developing cerebellum. Proc Natl Acad Sci U S A 108:9987–9992.

Henkart M, Landis DM, Reese TS (1976) Similarity of junctions between plasma membranes and endoplasmic reticulum in muscle and neurons. J Cell Biol 70:338 –347.

Holderith N, Lorincz A, Katona G, Ro´ zsa B, Kulik A, Watanabe M, Nusser Z (2012) Release probability of hippocampal glutamatergic terminals scales with the size of the active zone. Nat Neurosci 15: 988 – 997.

Ichikawa R, Miyazaki T, Kano M, Hashikawa T, Tatsumi H, Sakimura K, Mishina M, Inoue Y, Watanabe M (200) Distal extension of climbing fiber territory and multiple innervation caused by aberrant wiring to adjacent spiny branclets in cerebellar Purkinje cells lacking glutamate receptor GluRδ2. J. Neurosci 22: 8487 - 8503

Jun K, Piedras-Rentería, Smith SM, Wheeler DB, Lee SB, Lee TG, Chin H, Adams ME, Scheller RH, Tsien RW, Shin HS (1999) Ablation of P/Qtype Cav2.1 channel currents, altered synaptic transmission, and progressive ataxia in mice lacking the α1A-subunit. Proc Natl Acad Sci U S A 96:15245–15250.

Kakizawa S, Kishimoto Y, Hashimoto K, Miyazaki T, Furutani K, Shimizu H, Fukaya M, Nishi M, Sakagami H, Ikeda A, Kondo H, Kano M, Watanabe M, Iino M, Takeshima H (2007) Junctophilin-mediated channel crosstalk essential for cerebellar synaptic plasticity. EMBO J 26:1924 –1933.

Kasugai Y, Swinny JD, Roberts JD, Dalezios Y, Fukazawa Y, Sieghart W, Shigemoto R, Somogyi P (2010) Quantitative localisation of synaptic and extrasynaptic GABAA receptor subunits on hippocampal pyramidal cells by freeze-fracture replica immunolabelling. Eur J Neurosci 32:1868 –1888.

Kaufmann WA, Ferraguti F, Fukazawa Y, Kasugai Y, Shigemoto R, Laake P, Sexton JA, Ruth P, Wietzorrek G, Knaus HG, Storm JF, Ottersen OP (2009) Large conductance calcium-activated potassium channels in Purkinje cell plasma membranes are clustered at sites of hypolemmal microdomains. J Comp Neurol 515:215–230.

Kaufmann WA, Kasugai Y, Ferraguti F, Storm JF (2010) Two distinct pools of large-conductance calcium-activated potassium channels in the somatic plasma membrane of central principal neurons. Neuroscience 169:974 –986.

Kitano J, Nishida M, Itsukaichi Y, Minami I, Ogawa M, Hirano T, Mori Y, Nakanishi S (2003) Direct interaction and functional coupling between metabotropic glutamate receptor subtyoe 1 and voltage-sensitive Cav2.1 Ca^{2+} channel. J Biol Chem 278:25101–25108.

Kiyonaka S, Nakajima H, Takada Y, Hida Y, Yoshioka T, Hagiwara A, Kitajima I, Mori Y, Ohtsuka T (2012) Physical and functional interaction of the active zone protein CAST/ERC2 and the β-subunit of the voltage-dependent Ca^{2+} channel. J Biochem 152(2): 149-159.

Konnerth A, Dreesen J, Augustine GJ (1992) Brief dendritic calcium signals initiate long-lasting synaptic depression in cerebellar Purkinje cell. Proc. Natl. Acad. Sci 89: 7051-7055.

Kulik A, Nakadate K, Hagiwara A, Fukazawa Y, Luja´n R, Saito H, Suzuki N, Futatsugi A, Mikoshiba K, Frotscher M, Shigemoto R (2004) Immunocytochemical localization of the _1A subunit of the P/Q-type calcium channel in the rat cerebellum. Eur J Neurosci 19:2169 –2178.

Kurihara H, Hashimoto K, Kano M, Takayama C, Sakimura K, Mishina M, Inoue Y, Watanabe M (1997) Impaired parallel fiber 3 Purkinje cell synapse stabilization during cerebellar development of mutant mice lacking the glutamate receptor delta2 subunit. J Neurosci 17:9613–9623.

Lev-Ram V, Miyakawa H, Lasser-Ross N, Ross WN (1992) Calcium transients in cerebellar evoked by intracellular stimulation. J Neurophysiol 68:1167–1177.

Li L, Bischofberger J, Jonas P (2007) Differential gating and recruitment of P/Q-, N-, and R-type Ca2_ channels in hippocampal mossy fiber boutons. J Neurosci 27:13420 –13429.

Llinás R, Nicholson C (1971) Electrophysiological properties of dendrites and somata in alligator Purkinje cells. J Neurophysiol 34:532–551.

Llinás R, SugimoriM (1980) Electrophysiological properties of in vitro Purkinje cell dendrites in mammalian cerebellar slices. J Physiol 205:197–213.

Lörincz A, Nusser Z (2010) Molecular identity of dendritic voltage-gated sodium channels. Science 328:906 –909.

Lörincz A, Notomi T, Tama´s G, Shigemoto R, Nusser Z (2002) Polarized and compartment-dependent distribution of HCN1 in pyramidal cell dendrites. Nat Neurosci 5:1185–1193.

Luján R, Nusser Z, Roberts JD, Shigemoto R, Somogyi P (1996) Perisynaptic localization of metabotropic glutamate receptors mGluR1 and mGluR5 on dendrites and dendritic spines in the rat hippocampus. Eur J Neurosci 8:1488 –1500.

Magee JC (1998) Dendritic hyperpolarization-activated currents modify the integrative properties of hippocampal CA1 pyramidal neurons. J Neurosci 18:7613–7624.

Magee JC, Johnston D (1995) Synaptic activation of voltage-gated channels in the dendrites of hippocampal pyramidal neurons. Science 268:301–304.

Masugi-Tokita M, Shigemoto R (2007) High-resolution quantitative visualization of glutamate and GABA receptors at central synapses. Curr Opin Neurobiol 17:387–393.

Masugi-Tokita M, Tarusawa E, Watanabe M, Molna´r E, Fujimoto K, Shigemoto R (2007) Number and density of AMPA receptors in individual synapses in the rat cerebellum as revealed by SDS-digested freeze-fracture replica labeling. J Neurosci 27:2135–2144.

Matsubara A, Laake JH, Davanger S, Usami S, Ottersen OP (1996) Organization of AMPA receptor subunits at a glutamate synapse: a quantitative immunogold analysis of hair cell synapses in the rat organ of Corti. J Neurosci 16:4457– 4467.

Mintz IM, Sabatini BL, Regehr WG (1995) Calcium control of transmitter release at a cerebellar synapse. Neuron 15:675– 688.

Miyazaki T, Fukaya M, Shimizu H, Watanabe M (2003) Subtype switching of vesicular glutamate transporters at parallel fibre-Purkinje cell synapse in developing mouse cerebellum. Euro J. Neurosci 17:2563-2572.

Miyazaki T, Hashimoto K, Shin HS, Kano M, WatanabeM (2004) P/Q-type Ca^{2+} channel α1A regulates synaptic competition on developing cerebellar Purkinje cells. J Neurosci 24:1734 –1743.

Miyazaki T, Yamasaki M, Hashimoto K, Yamazaki M, Abe M, Usui H, Kano M, Sakimura K, Watanabe M (2012) Cav2.1 in cerebellar Purkinje cells regulates competitive excitatory synaptic wiring, cell survival, and cerebellar biochemical compartmentalization. J Neurosci 32:1311–1328.

Montgomery JR, Meredith AL (2012) Genetic activation of BK currents in vivo generates bidirectional effects on neuronal excitability. Proc Natl Acad Sci U S A 109:18997–19002.

Napper RM, Harvey RJ (1988) Number of parallel fiber synapse on an individual Purkinje cell in the cerebellum of the rat. J Comp Neurol 274:168 –177.

Neher E (1998) Vesicle pools and Ca^{2+} microdomains: new tools for understanding their roles in neurotransmitter release. Neuron 20:389 –399.

Nishimura S, Takeshima H, Hofmann F, Flockerzi V, Imoto K (1993) Requirement of the calcium channel β subunit for functional conformation. FEBS Lett 324: 283-286.

Okubo Y, Kakizawa S, Hirose K, Iono M (2001) Visualization of IP(3) dynamics reveals a novel AMPA receptor-triggered IP(3) production pathway mediated by voltage-dependent Ca^{2+} influx in Purkinje cells. Neuron 32:113-122.

Palay S, Chan-Palay V (1974) Cerebellar cortex. New York: Springer.
Palkovits M, Magyar P, Szenta´gothai J (1971) Quantitative histological analysis of the cerebellar cortex in the cat. 3. Strucutral organization of the molecular layer. Brain Res 34:1–18.

Parajuli LK, Fukazawa Y, Watanabe M, Shigemoto R (2010) Subcellular distribution of α1G subunit of T-type calcium channel in the mouse dorsal lateral geniculate nucleus. J Comp Neurol 518:4362– 4374.

Pfenninger K, Akert K, Moor H, Sandri C (1972) The fine structure of freeze-fractured presynaptic membranes. J Neurocytol 1:129 –149.

Pouille F, Cavelier P, Desplantez T, Beekenkamp H, Craig PJ, Beattie RE, Volsen SG, Bossu JL (2000) Dendro-somatic distribution of calciummediated electrogenesis in Purkinje cells from rat cerebellar slice cultures. J Physiol 527:265–282.

Pragnell M, De Waard M, Mori Y, Tanabe T, Snutch TP, Campbell KP (1994) Calciym channel beta-subunit binds to a conserved motif in the I-II cytoplasmic linker of the alpha 1-subunit. Nature 368:67-70.

Raman IM, Bean BP (1999) Ionic currents underlying spontaneous action potentials in isolated cerebellar Purkinje neurons. J Neurosci 19:1663–1674.

Rancz EA, Ha¨usser M (2006) Dendritic calcium spikes are tunable triggers of cannabinoid release and short-term synaptic plasticity in cerebellar Purkinje neurons. J Neurosci 26:5428 – 5437.

Rancz EA, Ha¨usser M (2010) Dendritic spikes mediate negative synaptic gain control in cerebellar Purkinje cells. Proc Natl Acad Sci U S A 107:22284 –22289.

Ross WN, Lasser-Ross N, Werman R (1990) Spatial and temporal analysis of calcium dependent electrical activity in guinea pig Purkinje cell dendrites. Proc R Soc Lond 240:173–185.

Sausbier M, Hu H, Arntz C, Feil S, Kamm S, Adelsberger H, Sausbier U, Sailer CA, Feil R, Hofmann F, Korth M, Shipston MJ, Knaus HG, Wolfer DP, Pedroarena CM, Storm JF, Ruth P (2004) Cerebellar ataxia and Purkinje cell dysfunction caused by Ca^{2+}-activated K^{+} channel deficiency. Proc Natl Acad Sci U S A 101:9474 –9478.

Takeshima H, Komazaki S, Nishi M, Iino M, Kangawa K (2000) Junctophilins: a novel family of junctional membrane complex protein. Mol Cell 6:11–22.

Tanaka J, Matsuzaki M, Tarusawa E, Momiyama A, Molnar E, Kasai H, Shigemoto R (2005) Number and density of AMPA receptors in single synapses in immature cerebellum. J Neurosci 25:799–807.

Tank DW, Sugimori M, Connor JA, Llina´s RR (1988) Spatially resolved calcium dynamics of mammalian Purkinje cells in cerebellar slice. Science 242:773–777.

Tarusawa E, Matsui K, Budisantoso T, Molna´r E, Watanabe M, Matsui M, Fukazawa Y, Shigemoto R (2009) Input-specific intrasynaptic arrangements of ionotropic glutamate receptors and their impact on postsynaptic responses. J Neurosci 29:12896 –12908.

Walter JT, Alvin˜a K, Womack MD, Chevez C, Khodakhah K (2006) Decrease in the precision of Purkinje cell pacemaking cause cerebellar dysfunction and ataxia. Nat Neurosci 9:389 –397.

Walton PD, Airey JA, Sutko JL, Beck CF, Mignery GA, Su¨dhof T, Deerinck TJ, EllismanMH (1991) Ryanodine and inositol triphosphate receptors coexist in avian cerebellar Purkinje neurons. J Cell Biol 113:1145–1157.

Westenbroek RE, Sakurai T, Elliott EM, Hell JW, Starr TV, Snutch TP, Catterall WA (1995) Immunochemical identification and subcellular distribution of the _1A subunits of brain calcium channels. J Neurosci 15:6403– 6418.

Williams SR, Stuart GJ (2000) Action potential bakcpropagation and somato-dendritic distribution of ion channels in thalamocortical neurons. J Neurosci 20:1307–1317.

Wittemann S, Mark MD, Rettig J, Herlitze S (2000) Synaptic localization and presynaptic function of calcium channel beta 4-subunits in cultured hippocampal neurons. J Biol Chem 275: 37807-37814.

Womack M, Khodakhah K (2002) Active contribution of dendrites to the tonic and trimodal patterns of activity in cerebellar Purkinje neurons. J Neurosci 22:10603–10612.

Womack MD, Chevez C, Khodakhah K (2004) Calcium-activated potassium channels are selectively coupled to P/Q-type calcium channels in cerebellar Purkinje neurons. J Neurosci 24:8818–8822.

Xu-Friedman M, Harris KM, Regehr WG (2001) Three-dimensional comparison of ultrastructural characteristics at depressing and facilitating synapses onto cerebellar Purkinje cells. J Neurosci 21(17):6666-66672.

Zander JF, Mu¨nster-Wandowski A, Brunk I, Pahner I, Go´ mez-Lira G, Heinemann U, Gutie´rrez R, Laube G, Ahnert-Hilger G (2010) Synaptic and vesicular coexistence of vGluT1 and vGAT in selected excitatory and inhibitory synapses. J Neurosci 30:7634 –7645.

Figures and Legends

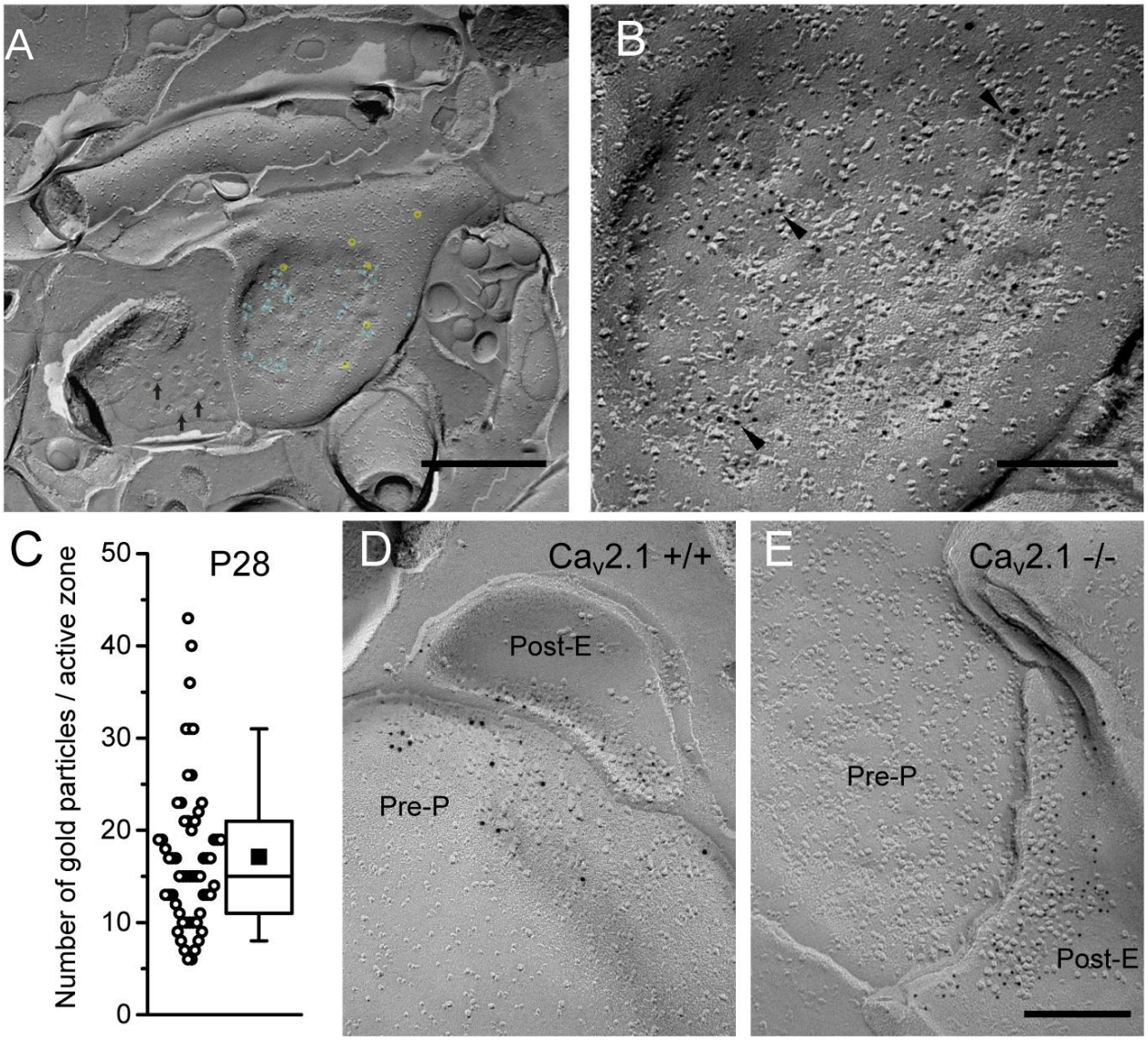

Figure 1 ***A***, The P-face and cross-fractured face of a parallel fiber bouton at P28 showing synaptic vesicles (arrows) and active zone indicated by concave shape of the P-face, high density of IMPs, and dimples (black arrowheads) representing vesicle exocytosis or endocytosis. This PF boutons was positive for $Ca_v2.1$ labeling (5nm, blue shades). PF boutons were identified with labeling for vGluT1 (10 nm particles, yellow shades). ***B***, Small clusters of immunogold particles for $Ca_v2.1$ (5 nm particles, arrowheads) were found within the active zone structure. ***C***, High variability of number of $Ca_v2.1$ particles (range: 6–43) was found in PF boutons at P28. Box

chart shows fifth, 25th, 75th, and 95th percentiles, median (bar), and mean (square). ***D***, in the wild-type mice ($Ca_v2.1^{+/+}$), clustered gold particles for $Ca_v2.1$ (10 nm) were found at PF presynaptic active zone (P-face) with opposing postsynaptic sites (E-face) labeled for AMPA receptors (5 nm). ***E***, The immunogold labeling for $Ca_v2.1$ was abolished in the $Ca_v2.1$ KO mice ($Ca_v2.1^{-/-}$), while AMPA receptor labeling (5 nm) remained. Scale bars: ***A***, 500 nm; ***B–E***, 200 nm.

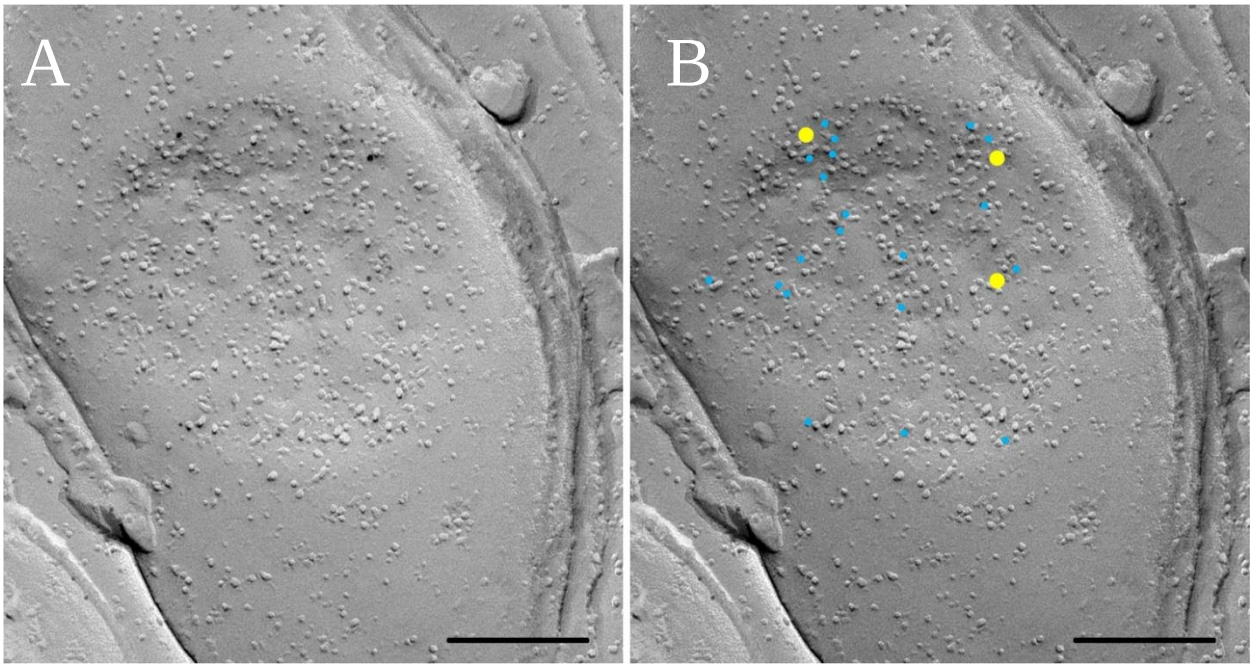

Figure 2 A-B Positive labeling for $Ca_v2.1$ (5 nm gold particles, blue shades) was detected in climbing fiber zone profile. Climbing fiber active zone was identified with positive labeling for vGlUT2 **(**10 nm gold particles, blue shades).

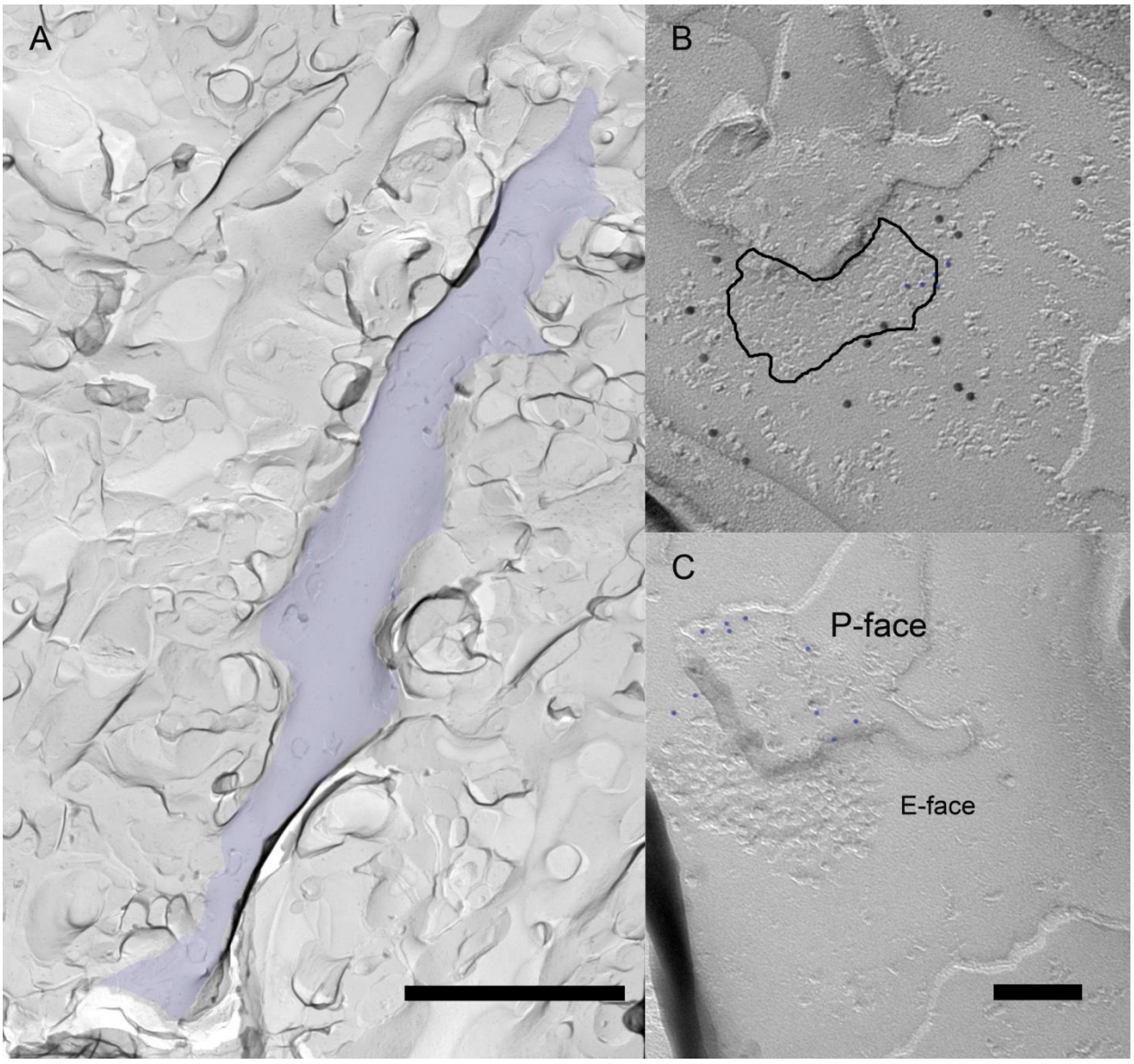

Figure 3 A, interneuron dendrite found in molecular layer (blue shades). B, Labeling for $Ca_v2.1$ (5nm gold particles, blue shades) was detected in the edge of PSD. C, Labeling for $Ca_v2.1$ (5nm gold particles, blue shades) was detected in P-face of presynaptic profile making synapse with interneuron. Scale bars, A = 2 μm, B-C = 100nm.

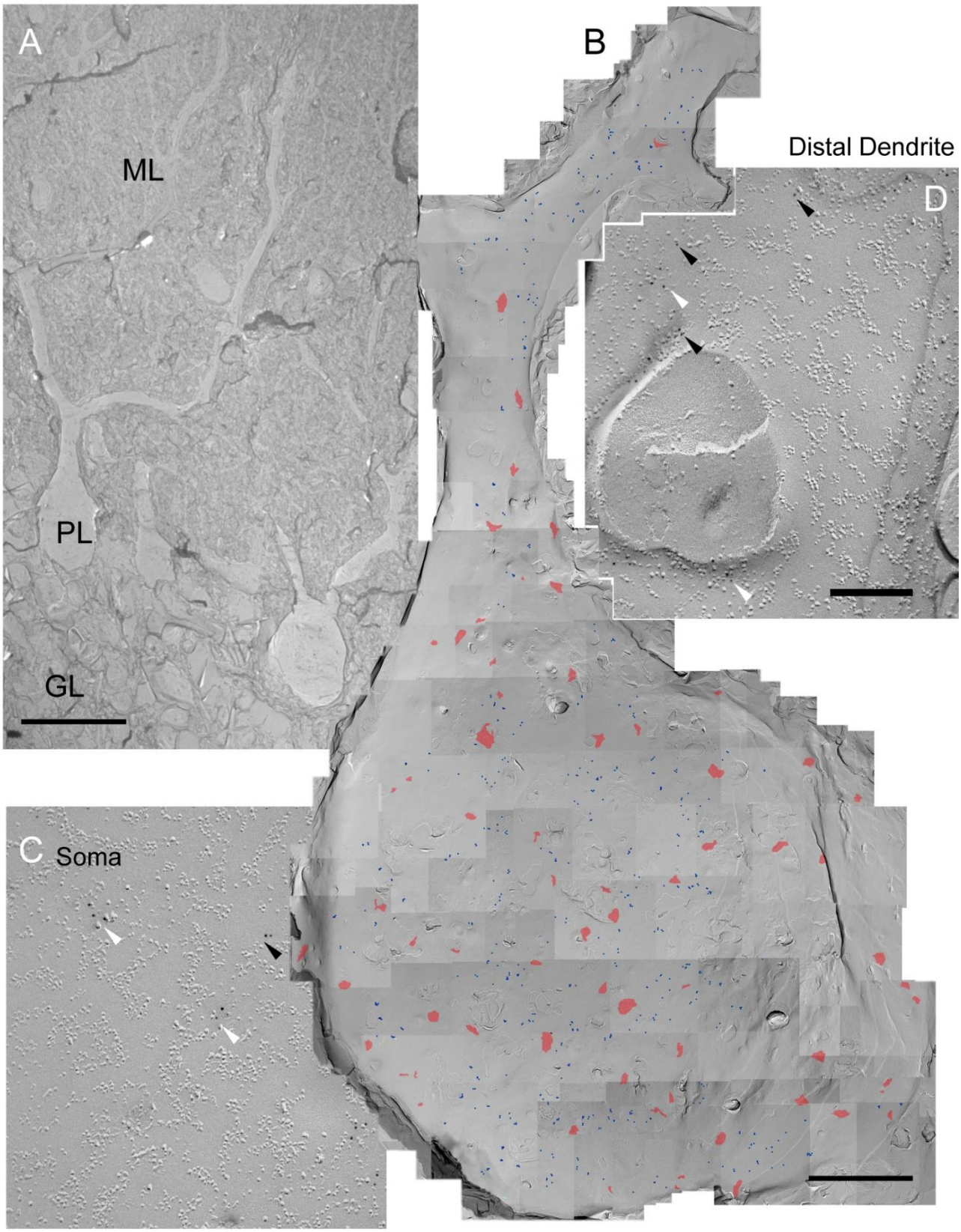
A
ML
PL
GL
B
Distal Dendrite
D
C Soma

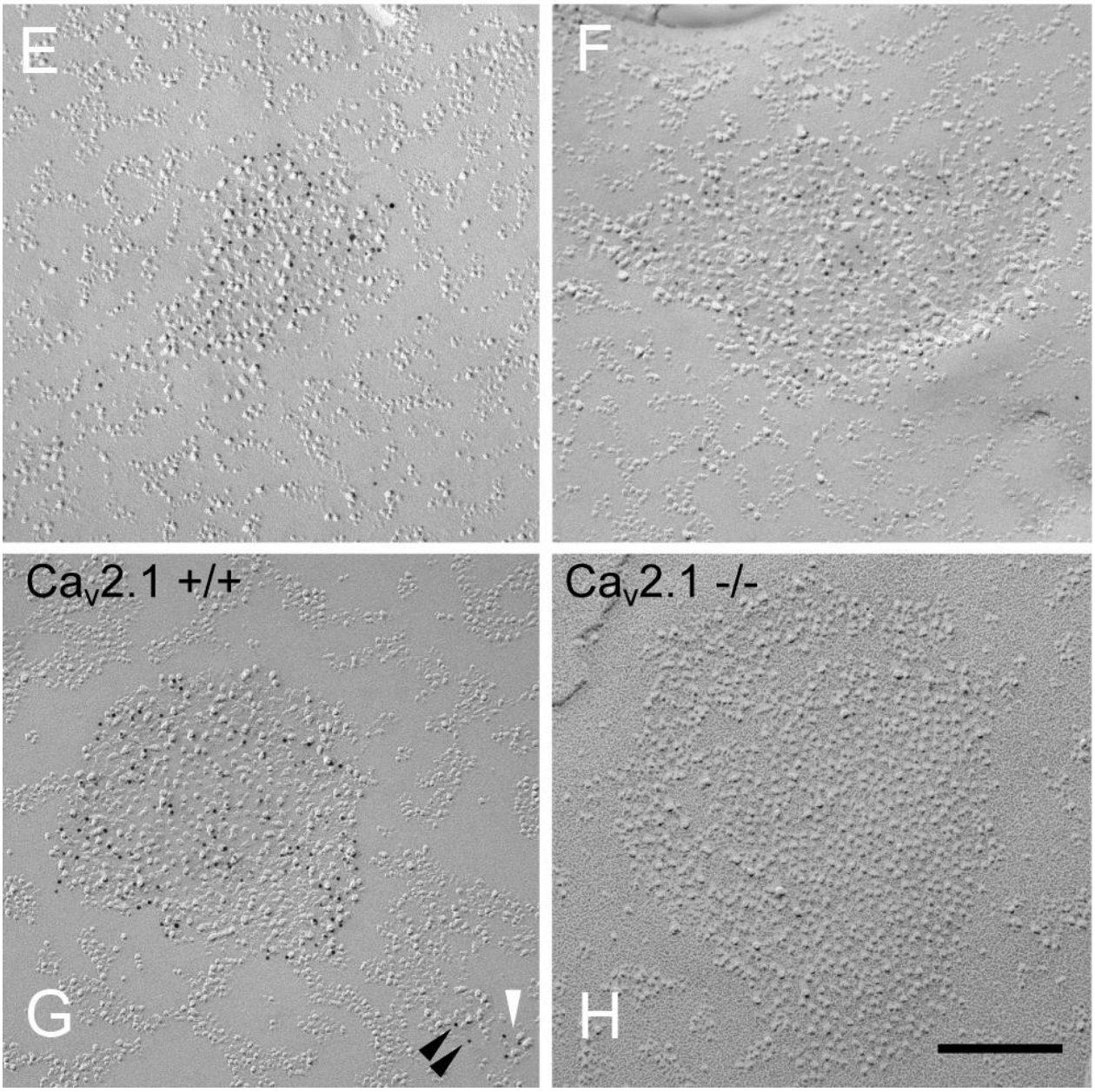

Figure 4 ***A***, The molecular layer (ML), Purkinje cell layer (PL), and granule cell layer (GL) are identifiable under low magnification of a replica image. ***B***, the P-face of soma and proximal dendrite of a PC labeled for $Ca_v2.1$ (5 nm). Immunogold particles for $Ca_v2.1$ were found concentrated within IMP clusters (red) and scattered throughout the plasma membrane (blue). The $Ca_v2.1$-labeled IMP clusters were diffusely distributed in the soma and proximal dendrite. ***C***,

D, scattered $Ca_v2.1$ particles in soma (***C***) and distal dendrites (***D***) showing isolated particles (black arrowheads) and small aggregations (white arrowheads). ***E***, ***F***, Clusters of immunogold particles for $Ca_v2.1$ were associated with IMP clusters. ***G***, The two distinct patterns of $Ca_v2.1$ localization, clustered and scattered (black arrowheads for isolated particles and a white arrowhead for a small aggregation), were also seen in wild-type mice. ***H***, The labeling for $Ca_v2.1$ within and outside of IMP clusters was absent in Cav2.1 KO mice. Scale bars: ***A***, 50µm; ***B***, 5 µm; ***C***, ***D***, 100 nm; **E–H**, 200 nm.

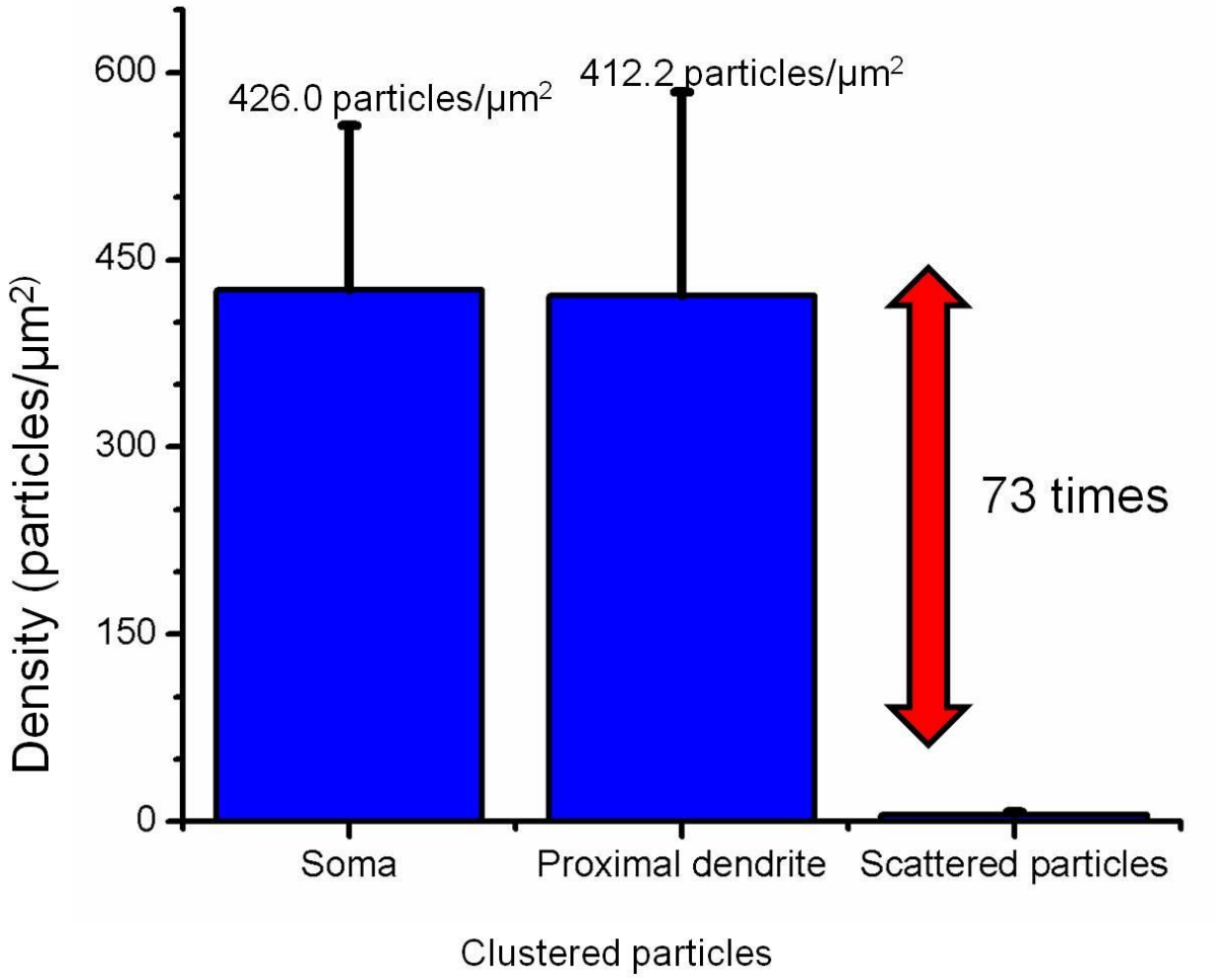

Figure 5 The $Ca_v2.1$ immunoparticle density within the IMP clusters was 73 times higher soma, 426.0 ± 131.3 particles/ μm^2, *n* = 73; proximal dendrite, 421.2 ± 163.2 particles/ μm^2, *n* = 40) than the density of the scattered particles (5.8 ± 1.68 particles/ μm^2, *n* = 4 in soma).

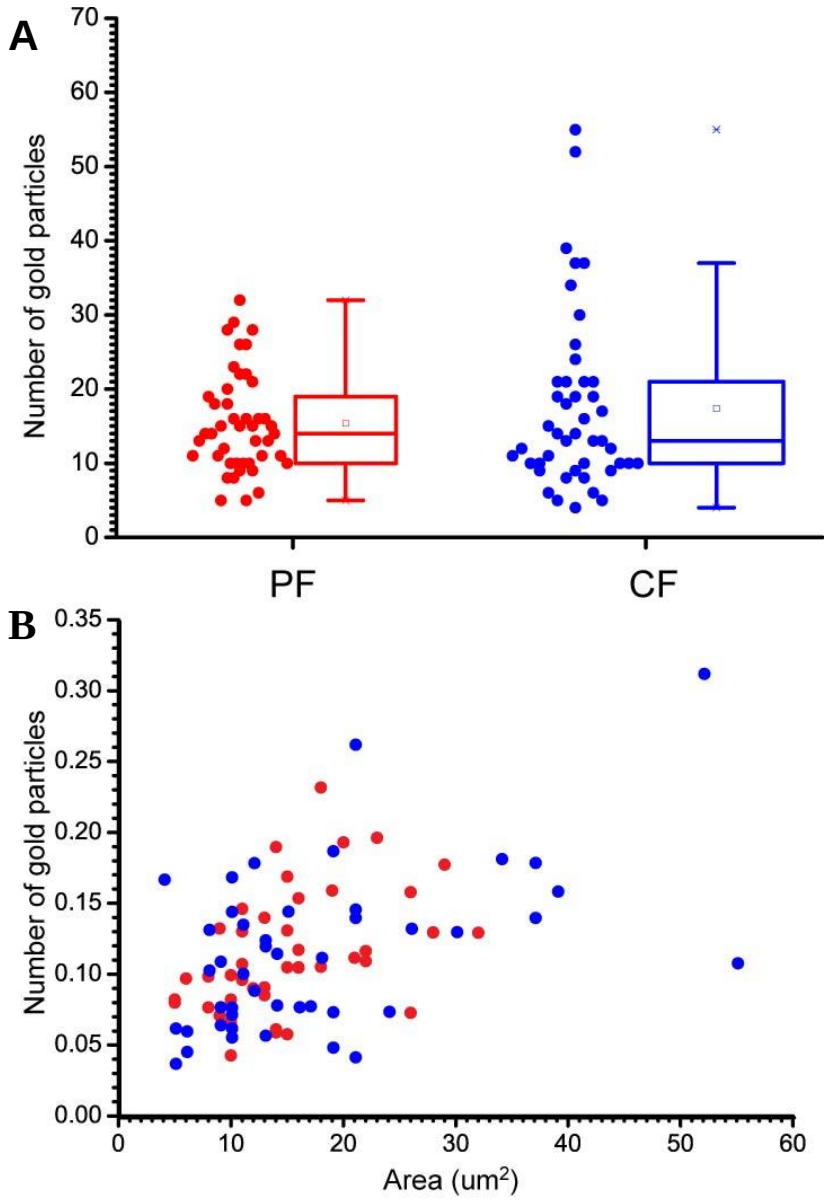

Figure 6 A,Similar number of $Ca_v2.1$particles was found in PF and CF. Box chart shows fifth, 25th, 75th, and 95th percentiles, median (bar), and mean (square). B,positive correlation between number of $Ca_v2.1$particles and active zone area seen in PF (red circles) and CF (blue circles).

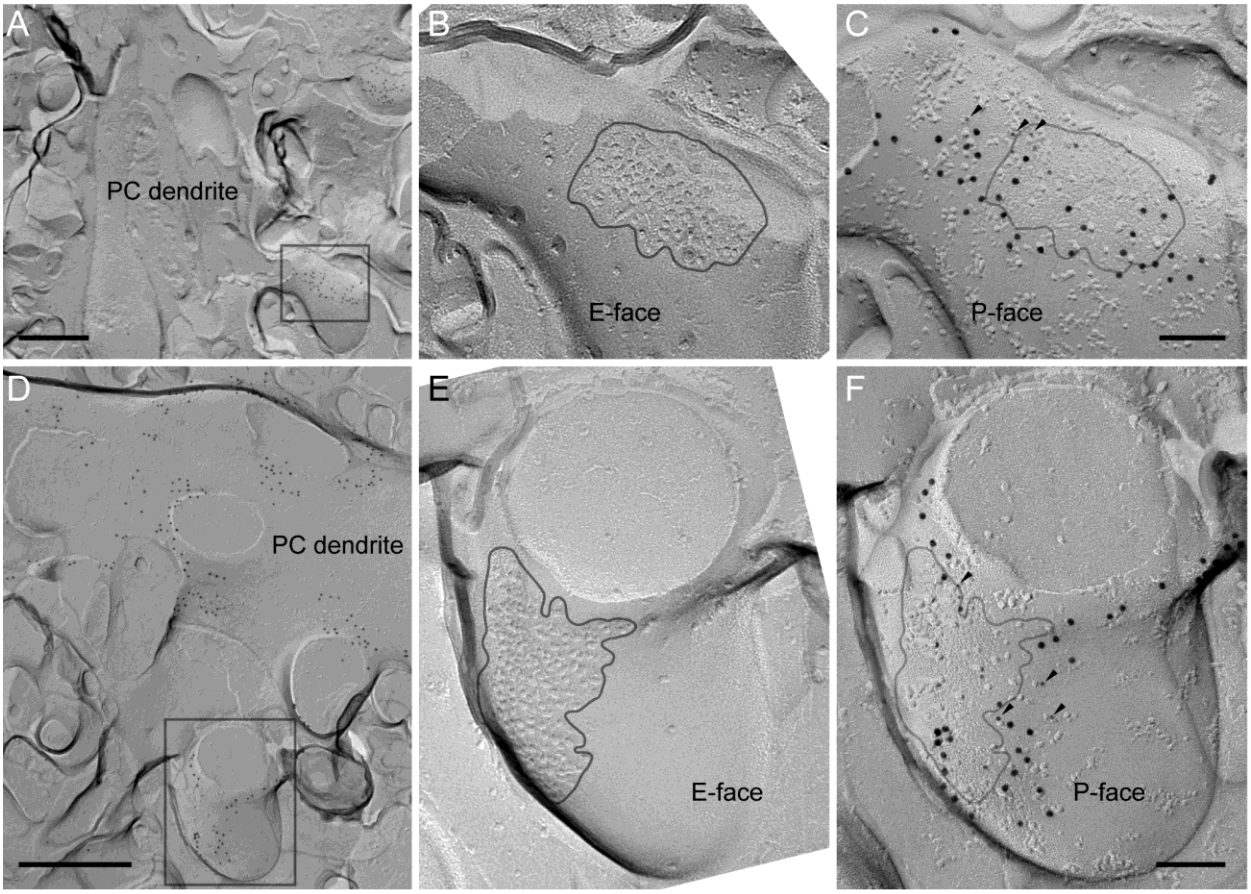

Figure 7 ***A***, ***D***, Low-magnification pictures showing spines protruding from PC dendrites. Areas in boxes are magnified in ***C*** and ***F***. These areas show the P-face of PC spines. ***B***, ***E***, Corresponding locations to the boxed areas in ***A*** and ***D*** were searched on the complimentary replica. The E-face of the spines had IMP clusters indicative of excitatory postsynaptic structure. Gray lines indicate the boundaries of synapses. Note that the corresponding replicas appear as mirrored images, thus one of the pictures (showing the E-face of synapses) was flipped to allow straightforward comparison with the other (***C***, ***F***, showing the P-face of the same synapse). In ***C*** and ***F***, the boundaries of the synapse determined in the E-face replica (***B***, ***E***) were projected onto the P-face. Labelings for mGluR1α (10 nm) and $Ca_v2.1$ (5 nm, arrowheads) were found colocalized near the boundary of the synapse. Scale bars: ***A***, ***D***, 500 nm; ***B***, ***C***, ***E***, ***F***, 100 nm.

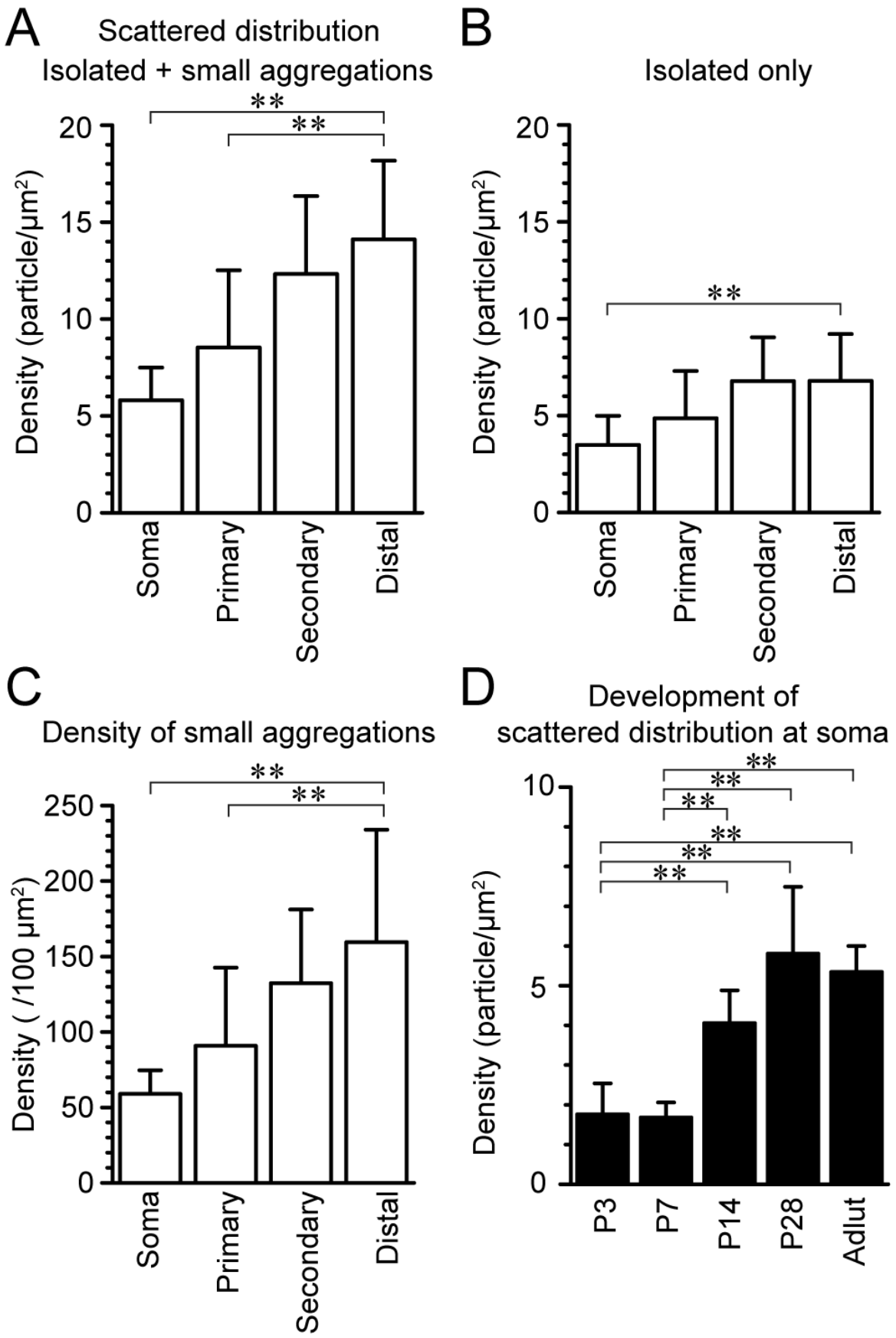
A
Scattered distribution
Isolated + small aggregations
Density (particle/μm²)
20
15
10
5
0
**
**
Soma
Primary
Secondary
Distal
B
Isolated only
Density (particle/μm²)
20
15
10
5
0
**
Soma
Primary
Secondary
Distal
C
Density of small aggregations
Density (/100 μm²)
250
200
150
100
50
0
**
**
Soma
Primary
Secondary
Distal
D
Development of
scattered distribution at soma
Density (particle/μm²)
10
5
0
**
**
**
**
**
**
P3
P7
P14
P28
Adlut

Figure 8 **A**, Density of the scattered $Ca_v2.1$particles (including both isolated particles and those within small aggregations) increased from soma to distal dendrites (soma = 5.81 ± 1.68 /μm^2; primary dendrite = 8.53 ± 3.99 /μm^2; secondary dendrite = 12.3 ± 4.01 /μm^2; distal dendrite = 14.1 ± 4.06 /μm^2; measured area = 700 –900μm2). ***B***, Out of all scattered $Ca_v2.1$ particles, the density of isolated particles only was extracted. The density increase from the soma to distal dendrites was also observed for the isolated particles (soma = 3.49 ± 1.50 / μm^2; primary dendrite = 4.86 ± 2.44 / μm^2; secondary dendrite = 6.78 ± 2.26 / μm^2; distal dendrite = 6.80 ± 2.41/ μm^2; measured area = 700 –900 μm^2). ***C***, The number of the small aggregation of $Ca_v2.1$ particles was counted and the density of such small aggregations was calculated. The density of the small aggregation also increased from soma to distal dendrites (soma = 59.0 ± 15.7/100 μm^2; primary dendrite = 90.9 ± 51.8/100 μm^2; secondary dendrite = 132.3 ± 48.9/100 μm^2; distal dendrite = 159.6 ± 74.4 / μm^2; measured area = 700 –900 μm^2, Kruskal–Wallis test, pairwise Mann–Whitney *U* test with Bonferroni correction). ***D***, Developmental increase of the density of scattered $Ca_v2.1$ particles was seen at PC soma after the second postnatal week (P3 = 1.76 ± 0.78 / μm^2; P7 = 1.68 ± 0.38 / μm^2; P14 = 4.06 ± 0.82 / μm^2; P28 = 5.81 ± 1.68 / μm^2; adult = 5.34 ± 0.65 / μm^2; measured area = 500 –1000 μm^2, ANOVA Tukey's test). * $p < 0.05$; ** $p < 0.01$.

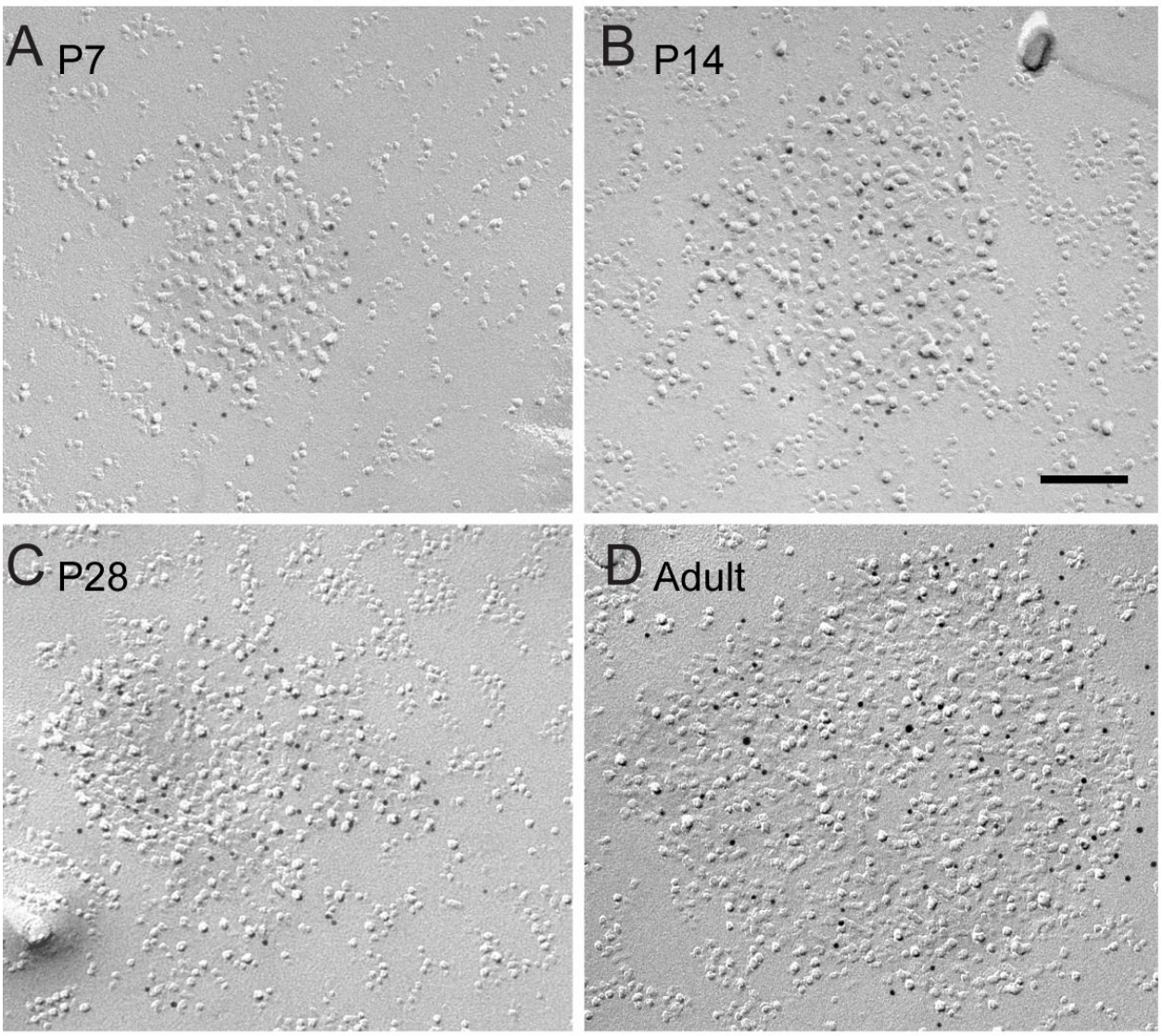
A P7
B P14
C P28
D Adult

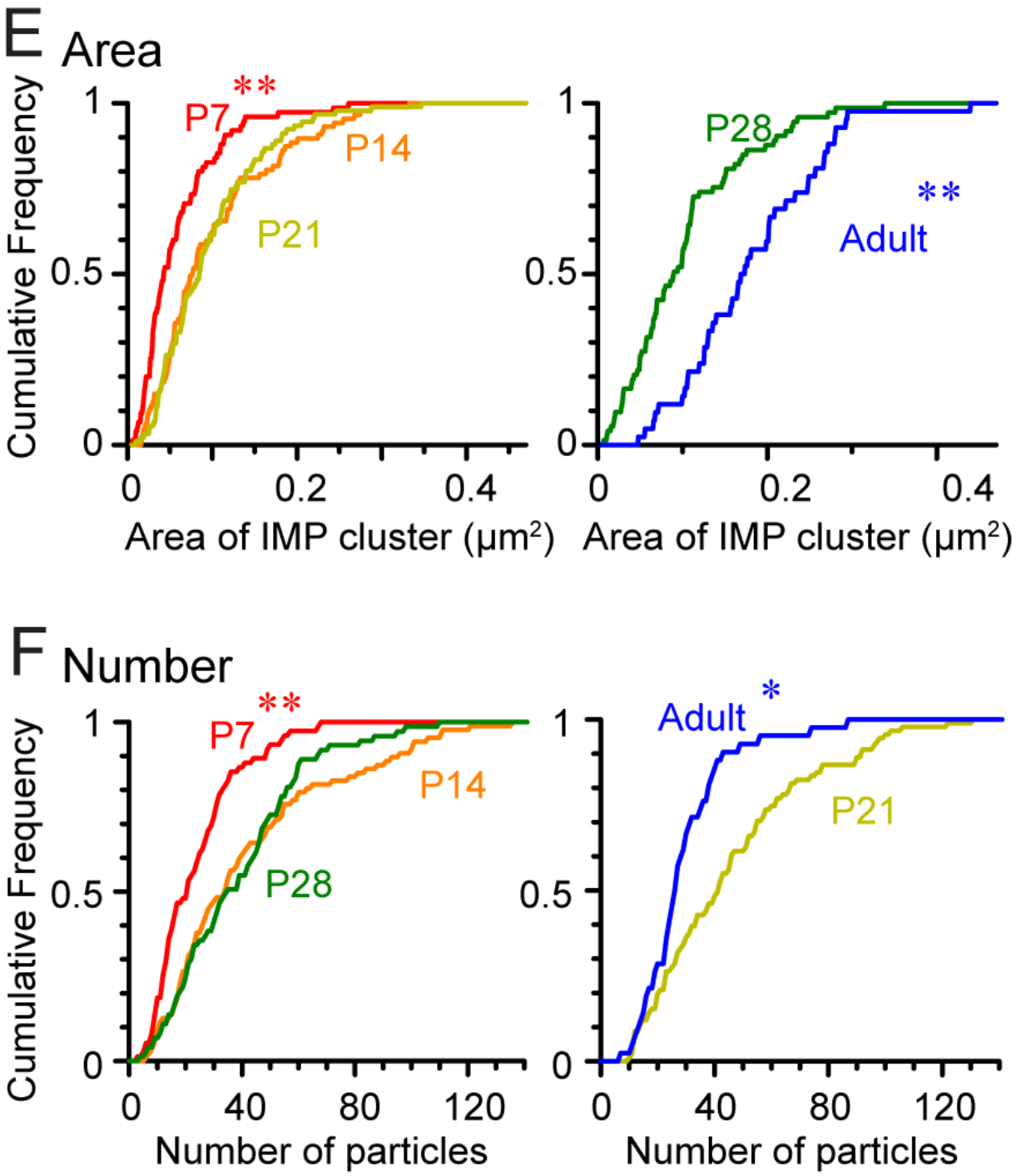
E
Area
Cumulative Frequency
1
0.5
0
0
0.2
0.4
Area of IMP cluster (μm²)
**
P7
P14
P21
P28
Adult
**
F
Number
Cumulative Frequency
1
0.5
0
0
40
80
120
Number of particles
**
P7
P14
P28
Adult
*
P21

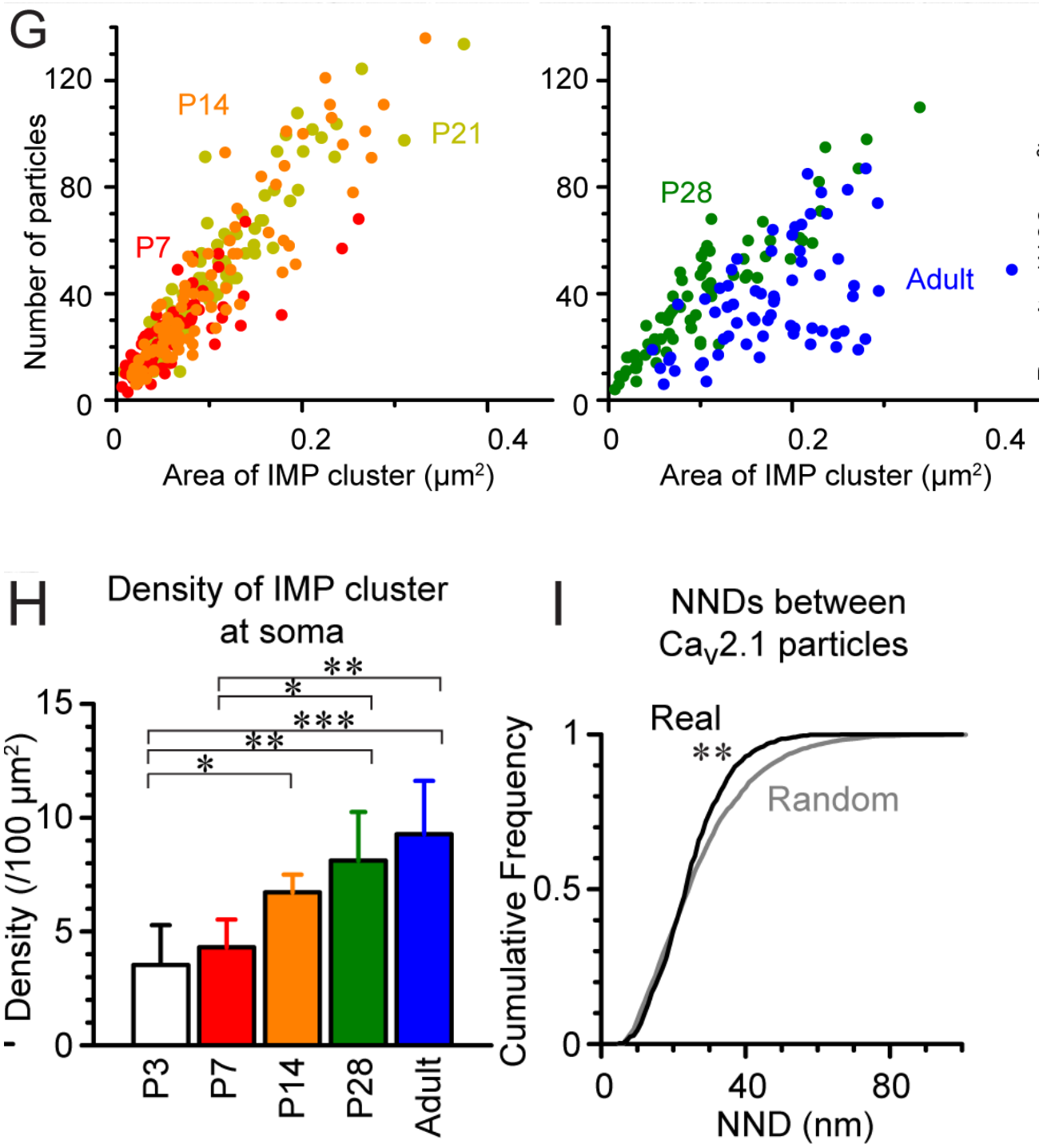
G
Number of particles
120
80
40
0
P14
P21
P7
0
0.2
0.4
Area of IMP cluster (μm²)
P28
Adult
H
Density of IMP cluster at soma
Density (/100 μm²)
15
10
5
0
**
*
***
**
*
P3
P7
P14
P28
Adult
I
NNDs between Cav2.1 particles
Cumulative Frequency
1
0.5
0
Real
**
Random
0
40
80
NND (nm)

Figure 9 **A–*D***, P-face IMP clusters labeled for $Ca_v2.1$ at P7 (***A***), P14 (***B***), P28 (***C***), and adult (***D***). ***E***, ***F***, Cumulative frequency plots for the IMP cluster size (***E***) and number of $Ca_v2.1$ particles within each IMP cluster (***F***). Significant differences in the IMP cluster size was observed between P7 and P14 and between P28 and adult. The number of $Ca_v2.1$ particles was significantly increased from P7 to P28, and decreased from P21 to adult (IMP cluster size: P7 = 0.060 ± 0.043 μm^2; P14 = 0.101 ± 0.077 μm^2; P21 = 0.097 ± 0.085 μm^2; P28 = 0.103 ± 0.090 μm^2; adult = 0.181 ± 0.171 μm^2; number of $Ca_v2.1$ particles; P7 = 23.8 ± 21.0 particles; P14 = 42.6 ± 34.0 particles; P21 = 46.3 ± 42.0 particles; P28 = 38.9 ± 35.0 particles; adult = 29.4 ± 26.5 particles; Kruskal–Wallis, pairwise Mann–Whitney *U* test with Bonferroni correction). ***G***, Positive correlation was found between the number of $Ca_v2.1$ particles and the IMP cluster size in all observed ages. The IMP cluster size and the number of $Ca_v2.1$ particles concurrently increased, thus the density (signified in the slope of the scattered plots) remained similar from P7 to P28 but significantly reduced in adult. ***H***, Density of IMP clusters increased in PC soma during postnatal development (P3 = 3.53 ± 1.75 clusters/100 μm^2; P7 = 4.51 ± 1.22 clusters/100 μm^2; P14 = 6.72 ± 0.78 clusters/100 μm^2; P28 = 8.12 ± 2.13 clusters/100 μm^2; adult = 9.28 ± 2.35 clusters/100 μm^2; ANOVA with Tukey's test). ***I***, Cumulative frequency plots of NNDs of $Ca_v2.1$ particles within the IMP cluster (Real) and randomly distributed NNDs generated using the same numbers of particles and IMP cluster areas (Random). The real NND was significantly smaller than the random NND, indicating clustering of $Ca_v2.1$ within the IMP cluster. $*p < 0.05$, $**p < 0.01$, $***p < 0.000$

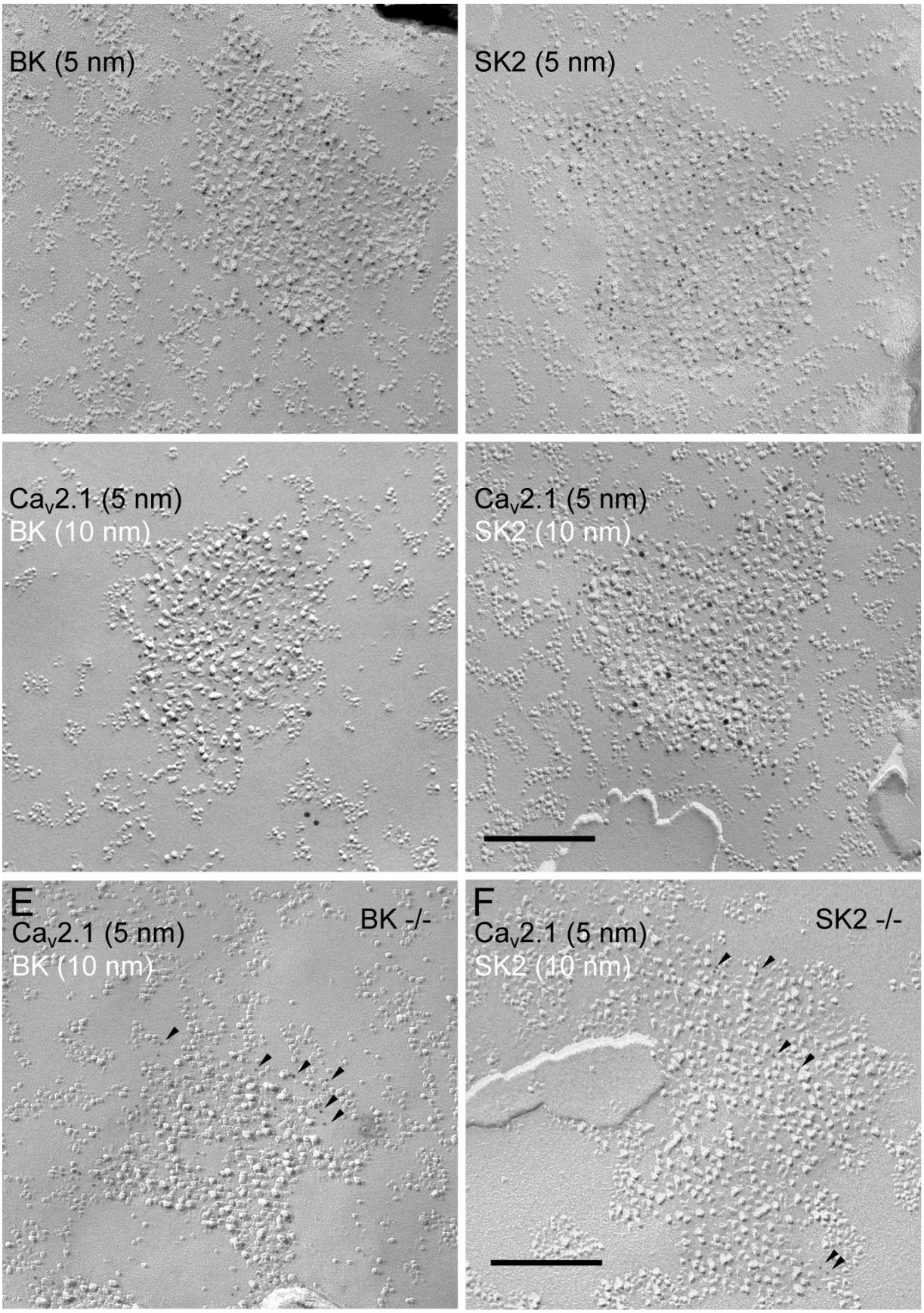
BK (5 nm)
SK2 (5 nm)
$Ca_v2.1$ (5 nm)
BK (10 nm)
$Ca_v2.1$ (5 nm)
SK2 (10 nm)
E
$Ca_v2.1$ (5 nm)
BK (10 nm)
BK -/-
F
$Ca_v2.1$ (5 nm)
SK2 (10 nm)
SK2 -/-

Figure 10 ***A***,***B***, Single labeling for BK or SK2 channels in the PC soma showing concentrated particles within the P-face IMP clusters. ***C***, ***D***, Double labeling for Cav2.1 (5 nm, black arrowheads) and either BK (10 nm, white arrowheads) or SK2 (10 nm, white arrowheads) channels revealed that these KCa channels are colocalized with Cav2.1 in the IMP clusters at PC soma. ***E***, ***F***, Double labeling for Cav2.1 (5 nm) and either BK (10 nm) or SK2 (10 nm) in BK KO (***E***) or SK2 KO (***F***) mice, respectively. The labeling for BK and SK2 channels disappeared in the respective KO mice verifying the labeling specificity. Labeling for Cav2.1 persisted in the IMP clusters in both KO mice. Scale bar, 200 nm.

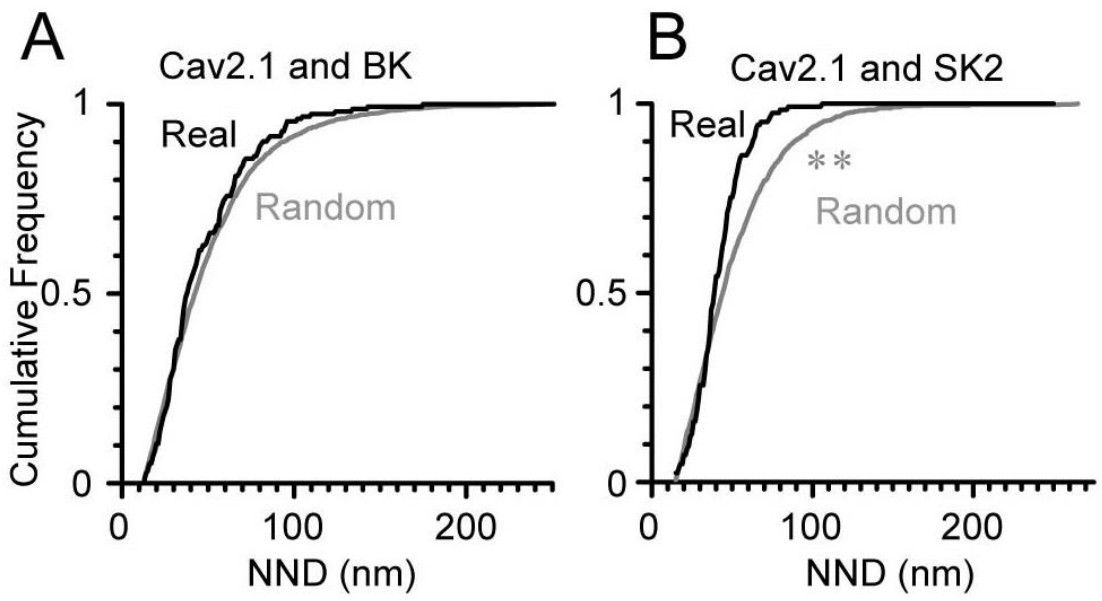

Figure 11 ***A***, ***B***, NNDs between BK (***A***) or SK2 (***B***) and Cav2.1 particles within the P-face IMP clusters were analyzed. In both cases, median of NND was quite small (~40 nm) suggesting calcium nanodomain formation. These NNDs (Real) were compared with randomly distributed NNDs (Random) generated using the same numbers of BK or SK2 particles same IMP cluster areas. The real NNDs were significantly smaller than the random NNDs for Cav2.1 and SK2 ($p = 0.019$, Man–Whitney U test, $p = 0.001$, Kolmogorov– Smirnov test) but not for Cav2.1 and BK.

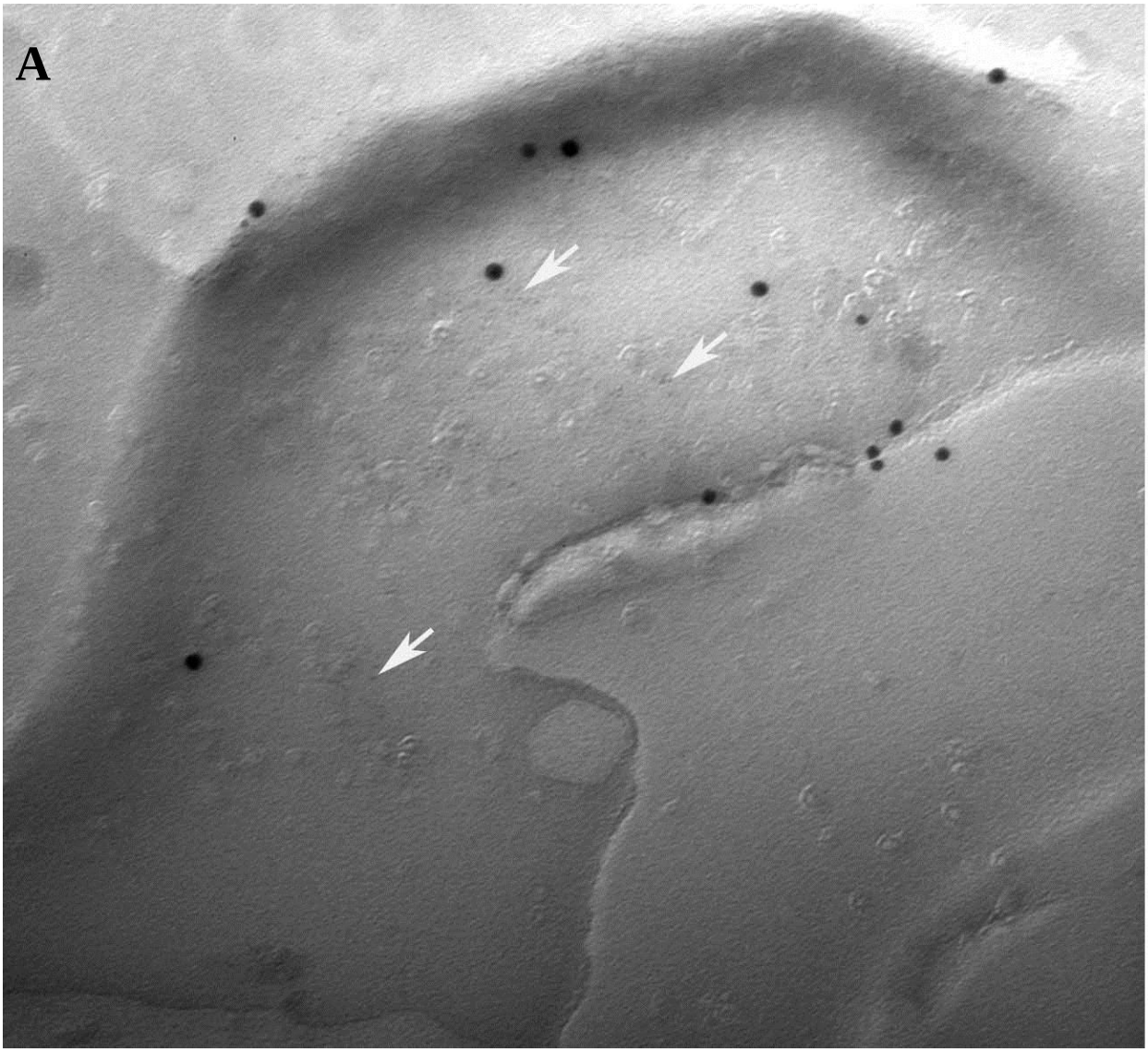
A

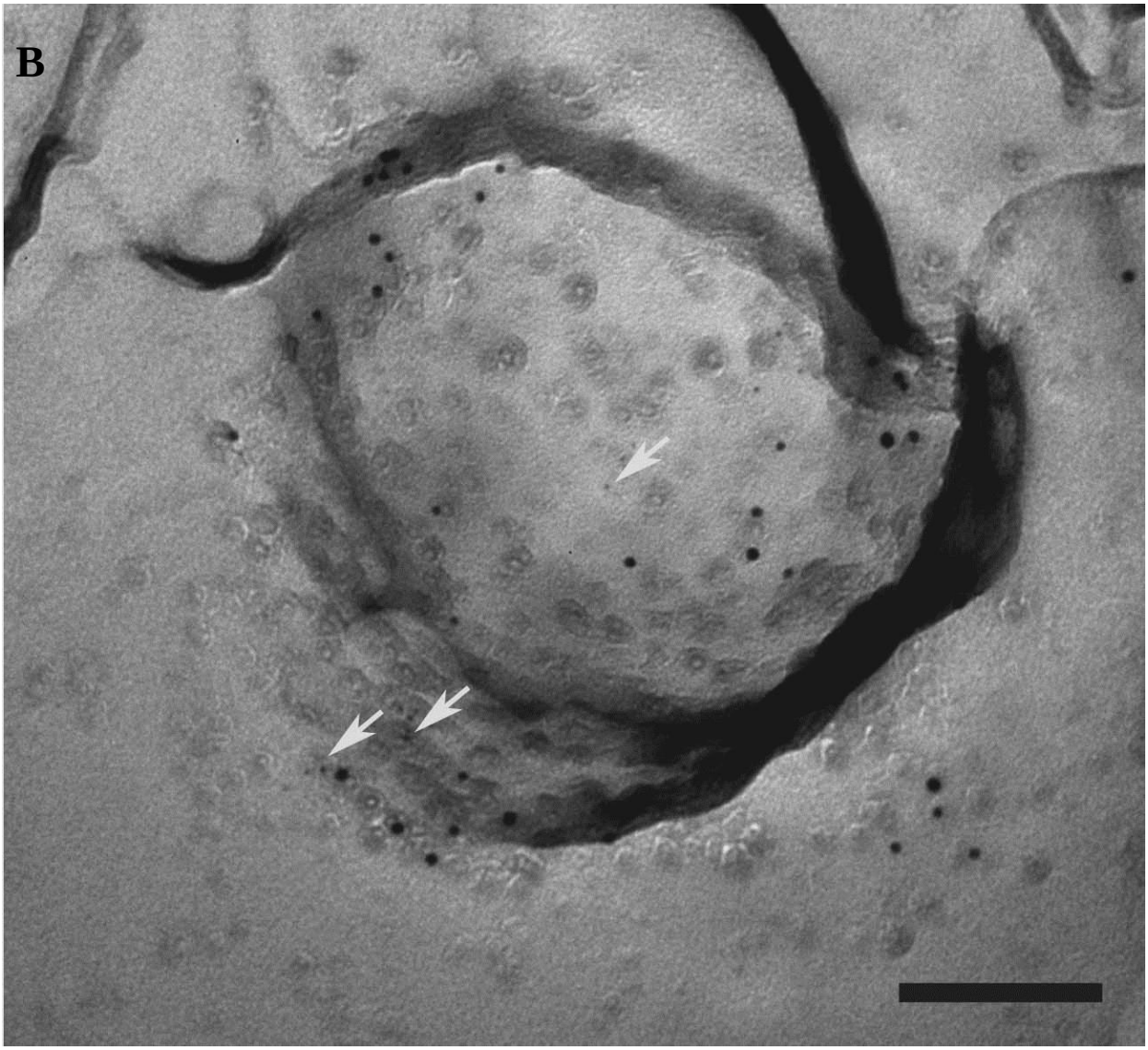

Figure 12 ***A***, The P-face of a parallel fiber bouton at adult rat showing synaptic vesicles (black arrows) and active zone indicated by concave shape of the P-face. This PF bouton was positive for β_4 and $Ca_v2.1$ labeling (5 nm and 2 nm, respectively). ***B,*** While in this PF bouton, β_4 was labeled with 2 nm gold particles and $Ca_v2.1$ was labeled with 5 nm gold particles. White arrows represent 2 nm gold particles. Scale bar, A - B = 100nm.

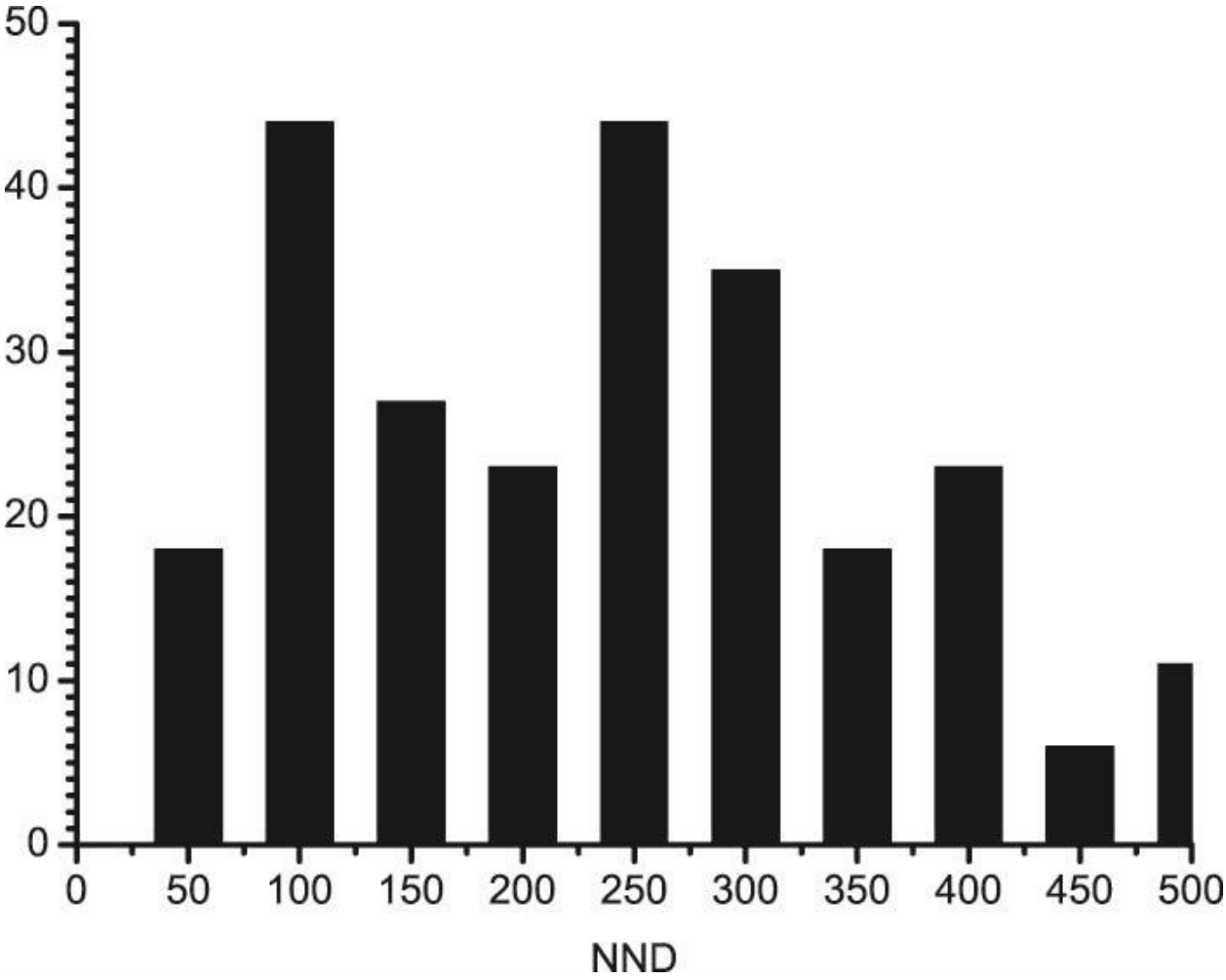

Figure 13 NND measured between $Ca_v2.1$ (5nm) and β_4 (2 nm) in PF active zone. Interquartile range 100.5 – 295 nm.